Low-Cycle Fatigue of Buckling Restrained Braces in Bidirectional Ductile End Diaphragms Due to Temperature-Change Effect on Bridge Superstructure

Xiaone Wei[1]; Luna Ngeljaratan[2]; and Michel Bruneau, F.ASCE[3]

Abstract: In bidirectional ductile end diaphragm systems (EDSs) in which buckling restrained braces (BRBs) are used as the hysteretic devices to provide ductile responses to earthquake excitations, BRBs that connect the abutments to the bridge's superstructure span across the expansion joints. Therefore, these BRBs should not only be designed to resist significant forces from seismic excitations, but would also be expected to accommodate the displacements due to the expansion or contraction of the bridge as a consequence of temperature changes. Such displacement demands on the BRBs would produce cyclic stresses and strains in the BRB's core plate, and the BRB must be designed to ensure that the low-cycle fatigue of the BRB is prevented over the design life of the bridge (or periodically replaced if having shorter low-cycle fatigue life). In the absence of such a consideration, BRBs would have to be connected to the abutment in series with lock-up devices to allow thermal expansion and contraction of the bridge under normal conditions but engaged during earthquakes, which is not a desirable detail. In this study, the low-cycle fatigue analyses of BRBs across bridge expansion joints are performed by subjecting a bridge to temperature changes from various cities to determine recommended design parameters. Resulting from these analyses, the minimum ratio of BRBs' core plate yielding length over total bridge length is recommended as 3% to avoid low-cycle fatigue over 75 years of thermal changes on the bridge superstructure.
DOI: 10.1061/(ASCE)BE.1943-5592.0001365.

Author keywords: Buckling restrained braces (BRBs); Low-cycle fatigue; Bidirectional ductile end diaphragm; Thermal effect; Slab-on-girder bridges.

Introduction

For bridges with slab-ongirder steel superstructures, the *AASHTO Guide Specifications for LRFD Seismic Bridge Design* (AASHTO 2011) included provisions for the design of specially detailed ductile diaphragms as permissible earthquake-resisting elements (EREs) to resist earthquake acting in the bridge transverse direction. However, this structural concept must be combined with other approaches to address seismic excitations in the longitudinal direction. To overcome this limitation, Celik and Bruneau (2011) first introduced bidirectional ductile end diaphragm systems (EDSs) inserted in straight or skew slab-ongirder bridge superstructures to resist earthquake excitations from all horizontal directions. In the two proposed schemes of bidirectional ductile EDSs (i.e., geometrical layouts) presented in Fig. 1, buckling restrained braces (BRBs) were arrayed to provide ductile responses to all horizontal seismic forces. In those schemes, BRBs are connected to abutments and cross expansion joints; therefore, they should not only be designed to resist significant forces from seismic excitations, but would also be expected to accommodate the displacements due to the expansion or contraction of the bridge as a consequence of temperature changes. Such displacement demands on the BRBs would produce cyclic stresses and strains in BRBs under a bridge's thermal movements; in some instances, the stresses in the yielding core of the BRBs may exceed its yield strength, and low-cycle fatigue may be a concern. The BRBs should be designed to ensure that low-cycle fatigue is prevented over the design life of the bridge (or a significant part) with sufficient life left to also resist earthquake excitations. Thus, satisfactory performance of the BRBs requires knowledge of the effect of years of thermal strain cycles on BRBs.

Initially developed in Japan by the Nippon Steel Corporation in Tokyo in the mid-1980s, the main component of a BRB is the yielding steel core plate, which is surrounded by the casing outside the BRB core plate. The global buckling of the BRB's core plate can be prevented over its encased length. As illustrated in Fig. 2, which is a typical BRB, a separation gap with debonding agent is placed between the steel core and the casing to ensure independent axial deformation of the yielding core plate relative to the restraining casing. There exist many manufacturers of BRBs delivering devices with different designs, but generally, their components remain fairly consistent. BRBs have been studied extensively and are mostly implemented in building structures and a few bridges all over the world for more than 30 years. They are designed to provide stable and reliable energy dissipation through high hysteretic deformations and typically have relatively large ductility capacity (Clark et al. 2000; Iwata et al. 2003; Sabelli et al. 2003; Tsai et al. 2003; López and Sabelli 2004; Uang et al. 2004; Tremblay et al. 2006; Fahnestock et al. 2007; Bruneau et al. 2011). Numerical models of various types of BRBs have been built and finite-element analyses have been performed to better understand their hysteretic behaviors (Korzekwa and Tremblay 2009; López-Almansa et al. 2012; Budaházy and Dunai 2015).

[1]Civil Associate, Michael Baker International, Chicago, IL 60606 (corresponding author). Email: xiaonewe@buffalo.edu

[2]Graduate Research Assistant, Dept. of Civil and Environmental Engineering, Univ. of Nevada, Reno, NV 89557.

[3]Professor, Dept. of Civil, Structural, and Environmental Engineering, Univ. at Buffalo, Amherst, NY 14260.

Note. This manuscript was submitted on October 3, 2017; approved on September 25, 2018; published online on February 1, 2019. Discussion period open until July 1, 2019; separate discussions must be submitted for individual papers. This paper is part of the ***Journal of Bridge Engineering***, © ASCE, ISSN 1084-0702.

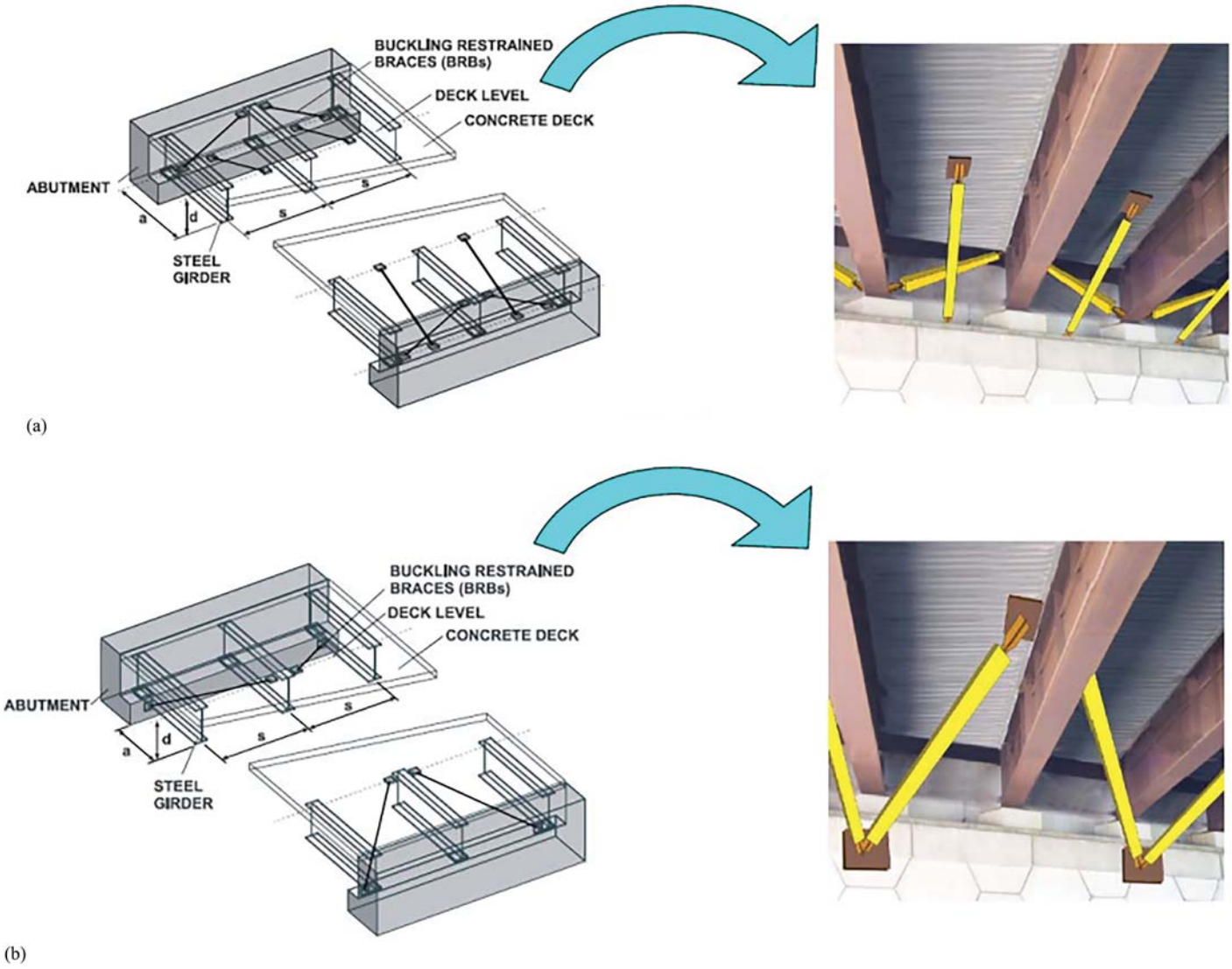

Fig. 1. Proposed schemes for bridge ductile end diaphragms: (a) EDS-1; and (b) EDS-2.

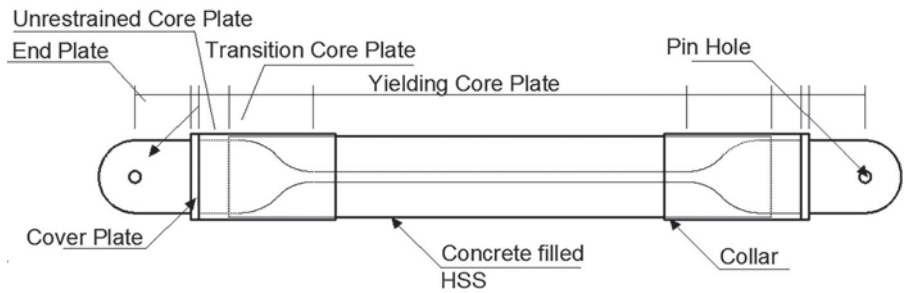

Fig. 2. Side view of a typical BRB specimen. HSS = hollow structural section.

Until now, only a few studies (Takeuchi et al. 2008; Usami et al. 2011; Wang et al. 2012a, b) have investigated the low-cycle fatigue of BRBs. Takeuchi et al (2008) investigated BRBs' low-cycle fatigue performance by using cumulative inelastic deformations, and they proposed equations to predict the cumulative absorbed energy and deformation capacities of BRBs based on assumed bilinear hysteretic behavior. Maeda et al. (1998), Nakamura et al. (2000), Usami et al. (2011), and Wang et al. (2012a, b) conducted experiments to show the comparisons of low-cycle fatigue performance of BRBs with different detailing, and the BRBs were all tested at constant strain amplitude, with strain ranges from 0.0004 to 0.08. However, no study has specifically addressed the low-cycle fatigue of BRBs in bridge applications spanning expansion joints and affected by bridge thermal expansion. Because BRBs in this case are subjected to strain histories with various amplitudes that change due to temperature fluctuation experienced by the BRBs every day,

this paper reports on research conducted to quantify the low-cycle fatigue life of BRBs in this bridge application. Note that bridge life is currently taken as 75 years by AASHTO (2014). Therefore, in addition to the seismic demands, the BRBs should be designed to be either left in place for 75 years, or plans could be made to periodically replace BRBs that have shorter low-cycle fatigue life. BRBs that fail to perform accordingly would have to be connected in series with lock-up devices to allow thermal expansion and contraction of the bridge under normal conditions. Also, these devices need to engage the BRBs during earthquakes, which would entail more complex and undesirable detailing. This study is intended as a first step toward establishing principles for the design of BRBs subjected to strain cycles as a consequence of temperature changes in this contemplated application.

The temperature change history and methodology considered in this study is presented. A simply supported bridge model is used to generate the strain histories for BRBs from temperature fluctuation data. Low-cycle fatigue analyses are conducted using the software Fatiga Version 1.03, and results on the BRBs' fatigue life are presented considering various temperature histories and ratios of the BRB's core length over the bridge's total length. The estimated fatigue life of BRBs obtained from Fatiga is solely based on the axial strain loading applied to the core plate steel. Because the core plate of a BRB typically develops local buckling under the applied low-cycle fatigue strain loading (albeit of constrained amplitude), this local buckling produces additional flexural plastic deformations that add up to the pure axial strains. A calibration factor was calculated to account for the fact that the local buckling of BRBs may reduce the estimated low-cycle fatigue life results.

Note that the BRBs in bidirectional EDSs are considered as secondary members, which, by definition (Marsh and Stringer 2013), are not part of the gravity load resisting system of the bridge under regular service condition, and it would only activate under seismic loads. There are only minimal forces in the BRBs due to vertical vehicular loads. Where the BRBs would be located, installed as envisioned, operational vehicular traffic would not produce significant differential axial or distortional deformations in the BRBs. In addition, the force in the BRBs due to braking forces caused by vehicular loads on the bridge is relatively small compared with the seismic force demand (Wei and Bruneau 2017, 2018). However, BRB designs should be checked to make sure that this is the case and that the BRB remains elastic (and at low-stress ranges) for the AASHTO (2014)-specified braking forces applied to the bridge. Per AASHTO 3.6.4, the braking force per lane can be calculated as the maximum force obtained from: (1) 25% of axle weights of the design truck/tandem and (2) 5% of design truck/tandem plus lane load. The resulting braking force per lane is 80 kN (18 kips). If a bridge has trucks in all lanes, and all trucks brake at the same time, all the BRBs at the ends would be subjected to this braking force times the number of lanes [for example, this would be 160 kN (36 kips) for a two lane bridge]. For a proper application of the proposed concept, the designer would need to verify that this braking force from the live load does not yield the BRBs. In addition, repeated applications of this design braking force over the bridge's lifetime may cause some stress cycles that, technically, would add to cycle counting as part of the fatigue life calculation. However, for the previous160 kN (36 kips) example, a yielding core with a cross sectional area of less than a square inch and yield strength of 289 MPa (42 ksi) would be sufficient to achieve elastic response and keep this contribution to fatigue within the realm of high-cycle fatigue for the BRBs (i.e., with little impact on the low-cycle fatigue calculations). Note that BRBs used for seismic response typically will require significantly greater cross sectional area in the yielding core. In other words, although the focus of study in this paper is about the effect of the temperature changes on the BRB design in bidirectional ductile diaphragm systems, the engineer is cautioned that future study on the fatigue of BRBs due to braking forces on the bridge may broaden the understanding of BRBs' behaviors in the bidirectional ductile diaphragm system. However, the authors believe that this issue is not expected to have a significant impact on fatigue life when the corresponding stresses remain well into the elastic range, in accordance with the design intent.

Summary of Experimental Results

The analytical results in this paper have been used to experimentally investigate the BRBs' behaviors in the bidirectional EDS application in Wei and Bruneau (2018). Eight BRB specimens were subjected to an extensive set of quasi-static experiments consisting of a regime of combined relative end displacement histories, representative of the displacement demands induced by earthquakes as well as the thermal changes on the bridges presented in this study. In one example relevant to the material presented, one BRB specimen resisted the design displacement histories corresponding to those induced by temperature change at the expansion joint of a representative bridge over 75 years in service without failure. To fail the specimen, additional cycles of displacement histories were applied by progressively scaling the displacement amplitude above those corresponding to the design temperature-induced displacement history. For the other BRBs that were tested under displacement demands corresponding to various combinations of design earthquake and years of thermal changes, the test results showed that the design seismic displacement demands caused significantly more damage (i.e., more cumulative inelastic displacements) than the temperature-induced displacement demands. However, the experiments also showed that low-cycle fatigue induced by the effect of temperature changes on the bridge can affect the BRB's service life (and this will be more significant for BRBs having shorter yielding core length). The capability of the BRBs to endure the inelastic displacement demands from earthquakes was reduced when considering the temperature-change effect. Based on the total low-cycle fatigue life empirically obtained from test results, it was recommended that BRBs installed in bridges be replaced after 35 years of service to ensure adequate performance under the expected seismic demands; guidance was provided to indicate how longer service life could be achieved. Information of the comprehensive experimental work and corresponding design and detailing recommendations are also presented in Wei and Bruneau (2018).

Temperature History and Background

In this study, the thermal expansions or contractions of bridges, resulting in strains on BRBs, were calculated from actual recorded maximum and minimum daily temperatures (AccuWeather 2012) for cities arbitrarily chosen to represent a broad selection of seismic regions and scenarios of daily and yearly temperature variations. The selected eight locations within the United States were Anchorage, Alaska; Boston; Charleston, South Carolina; Los Angeles; Memphis, Tennessee; Portland, Oregon; San Francisco; and Seattle. Quebec City in Canada was also chosen due to its wide range of temperature variations within a year and significant seismic sources near the city. The resulting temperature history for the city of Memphis is presented in Fig. 3, whereas the temperature histories for the other eight cities considered are presented in Fig. S1. For determining the thermal movement of bridges, AASHTO (2014) provided maximum and

minimum design temperatures that may result in a slightly larger range of demands for some of these locations. However, it must be recognized that AASHTO specified extreme temperature ranges that may happen only a few times over the life of the bridge for the purpose of calculating maximum effects in design, whereas the temperature history in Fig. 3 is applied to the bridge repeatedly each year for a considerably large number of cycles.

Because the thermal strain history applied to BRBs has variable amplitudes, strain cycles were computed using the rainflow counting method (Matsuishi and Endo 1968), which is commonly used to extract cycles from variable-amplitude loading. The resulting cyclic hystereses (i.e., stress–strain relationships) in the BRBs corresponding to the strain histories were generated using Ramberg-Osgood and Masing-Morrow models, which were used later to compute the low-cycle fatigue life.

The Ramberg-Osgood model (Ramberg and Osgood 1943), represented by Eq. (1), exhibits a nonlinear behavior from the beginning (i.e., from zero stress level). The model consists of a power law relation between stress, σ, and total strain, ε, in which the total strain consists in the sum of elastic and plastic strains

$$\varepsilon = \frac{\sigma}{E} + \left(\frac{\sigma}{K'}\right)^{1/n'} \tag{1}$$

where E = elastic modulus; K' = cyclic strength; and n' = cyclic strain hardening component.

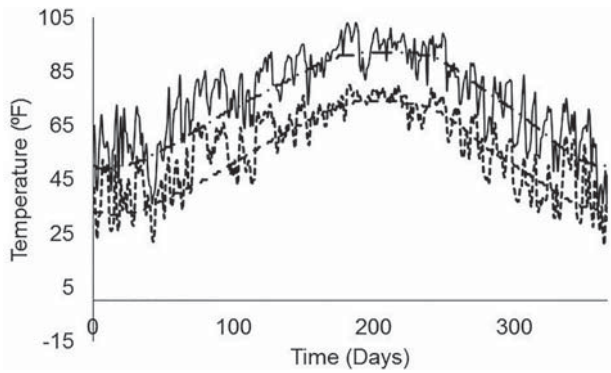

Fig. 3. Recorded temperature data for Memphis in 2012.

The Masing-Morrow model (Masing 1926; Morrow 1965), expressed in Eq. (2), was developed based on the observation that each branch of the hysteresis loop was geometrically similar to the monotonic stress–strain curve with a scale factor of two. On unloading and taking peak tensile load as the new origin, each element was required to deform through twice its previous equivalent yield stress, $2\sigma_y$. The tension path of the model followed the compression path resulting in a closed hysteresis loop:

$$\Delta\varepsilon = \frac{\Delta\sigma}{E} + 2\left(\frac{\Delta\sigma}{2K'}\right)^{1/n'} \tag{2}$$

The stress–strain hysteresis loops were generated as presented in Fig. 4, in which the first half cycle (i.e., inner loop) is assumed to follow the stable cyclic stress–strain response as expressed in the Ramberg-Osgood relationship in Eq. (1). The subsequent cyclic stress–strain hysteresis loops follow the Masing relationship in Eq. (2).

Three models were used to estimate the fatigue life of BRBs by considering or neglecting the mean stress effect: the Basquin-Coffin-Manson model (Basquin 1910; Coffin 1954; Manson 1954), the Smith-Watson-Topper model (Smith et al. 1970), and the Morrow model (Morrow 1968). The Basquin-Coffin-Manson model ignores the effect of mean stress on fatigue behaviors, whereas the latter two models have mean stress correction. Previous studies (Maeda et al. 1998; Nakagomi et al. 2000) have shown that such models could be applied to the BRB core plate assuming that plastic strains were generally distributed over the entire length of the core plates, that sufficient constraint against buckling was provided, and that the core plate maintained its positive incremental stiffness after yielding. Generally, the high-cycle, low-strain regime in which the nominal strains were elastic is expressed by Eq. (3)

$$\frac{\Delta\varepsilon_e}{2} = \frac{\sigma_f'}{E}(2N_f)^b \tag{3}$$

whereas the low-cycle, high-strain regime in which the nominal strains are plastic is described by Eq. (4)

$$\frac{\Delta\varepsilon_p}{2} = \varepsilon_f'(2N_f)^c \tag{4}$$

These two regimes of elastic and plastic strains are accumulated to give the total strain, providing the basic relationship between total strain range and cyclic life given in Eq. (5)

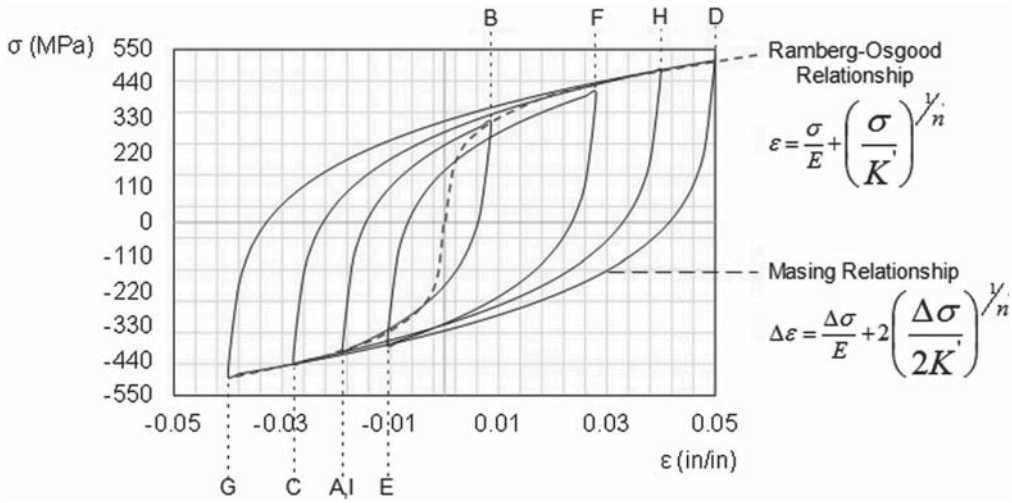

Fig. 4. Example of a stress–strain hysteresis loop.

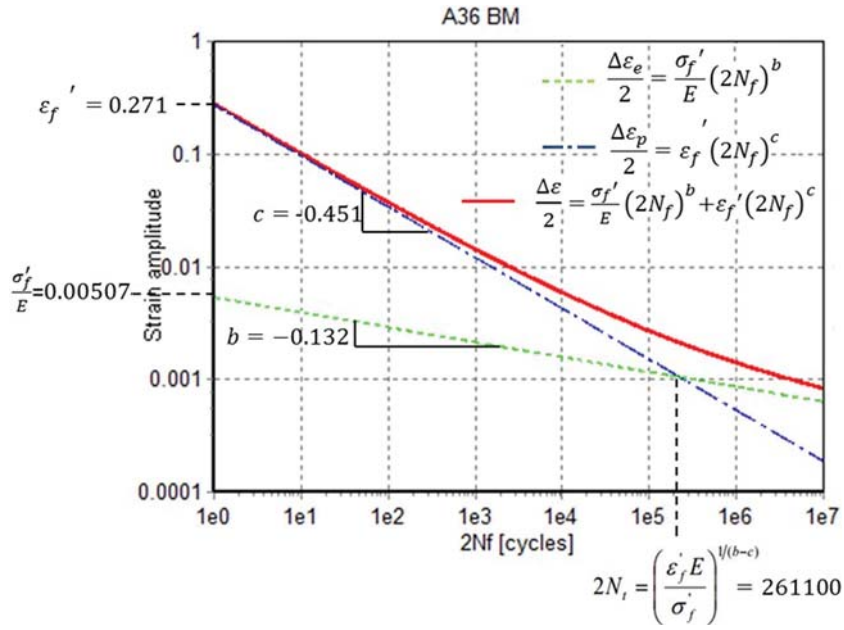

Fig. 5. Strain-life curve for ASTM A36 steel.

$$\frac{\Delta\varepsilon}{2} = \frac{\Delta\epsilon_e}{2} + \frac{\Delta\varepsilon_p}{2} = \frac{\sigma_f'}{E}(2N_f)^b + \varepsilon_f'(2N_f)^c \tag{5}$$

The strain-life curve in Fig. 5 was generated using the Basquin-Coffin-Manson model for ASTM (2017) A36 steel with the following material fatigue properties: elastic modulus E = 200,000 MPa, fatigue strength coefficient σ_f' = 1,014 MPa (147 ksi), fatigue strength exponent b = –0.132, fatigue ductility coefficient ε_f' = 0.271, fatigue ductility exponent c = –0.451, cyclic strength coefficient K' = 1,097, and cyclic strain hardening exponent n' = 0.249 (Higashida et al. 1978). The strain-life curve provides the relationship between the applied strain amplitude, $\Delta\varepsilon/2$, and the fatigue life reversals to failure, $2N_f$. Two reversals are equal to one cycle, and cycles to failure are presented as reversals to failure. Elastic strain amplitude, $\Delta\varepsilon_e/2$, is related to $2N_f$ by a linear relationship in Eq. (3) (in a log-log space) with a slope equal to the fatigue strength exponent, b, as illustrated by the dashed line in Fig. 5. The plastic strain amplitude, $\Delta\varepsilon_p/2$, is expressed in Eq. (4) as a linear function of $2N_f$ (in log-log space) of slope equal to the fatigue ductility exponent, c, as illustrated by the dashed-dot line in Fig. 5. The applied total strain amplitude (elastic plus plastic strain) corresponds to the solid line in Fig. 5. The life, in which elastic and plastic components of strain are equal, is called the transition fatigue life $(2N_t)$ and corresponds to 261,100 reversals for ASTM A36 steel. For lives less than $2N_t$, the deformation is mainly plastic; whereas for lives larger than $2N_t$, the deformation is mainly elastic.

Mean stress could have some influence on fatigue life and that the fatigue process is sensitive to tensile mean stress in both the high-cycle fatigue and low-cycle fatigue regimes (Stephens et al. 2001). For cases with low-strain amplitudes (<0.005), fatigue life increases or decreases if the mean stress is compressive or tensile, respectively (Koh and Stephens 1991), because the fatigue failure mechanism is due to the slip of atomic lattice planes (Osgood 1982), and mean compressive stress helps prevent the separation of atomic planes.

The Smith-Watson-Topper model in Eq. (6) assumes that the product of the maximum tensile stress, $\sigma_{\max}$, and the strain amplitude ε_a control and that a constant fatigue life is obtained if their product remains constant

$$\sigma_{\max}\varepsilon_a = \frac{(\sigma_f')^2}{E}(2N_f)^{2b} + \varepsilon_f'\sigma_f'(2N_f)^{b+c} \tag{6}$$

where $\sigma_{\max}$ = maximum stress of a given cycle. This method will predict an infinite fatigue life if the maximum tensile stress is zero or negative.

The Morrow model in Eq. (7) assumes that the mean stress had a more significant effect on the fatigue life when cycles of elastic strain amplitude dominate, and this only affects the elastic portion of the strain life

$$\frac{\Delta\varepsilon}{2} = \frac{\sigma_f' - \sigma_m}{E}(2N_f)^b + \varepsilon_f'(2N_f)^c \tag{7}$$

where σ_m = mean stress of a given cycle.

The damage caused by cycles at each amplitude is accumulated using the Palmgren-Miner rule (Palmgren 1924; Miner 1945), which assumes that the percentage of damage contributed by each cycle in a strain history at a specific range is independent from those produced over other ranges. Consequently, the failure condition of a material subjected to variable-amplitude loading is calculated using Eq. (8). Fatigue failure is achieved when this damage is equal to 1.0. For example, if a material is subjected to a certain number of cycles (or stress reversals) n_i of stress amplitude, s_i, and the total number of stress cycles to cause failure at that given amplitude level is N_{fi}, then the material has attained a partial fatigue damage of $D_i = n_i/N_{fi}$. For other stress amplitudes, the corresponding partial damage contributions can be calculated and summed to produce a total accumulated damage of D. It is assumed that failure occurs when $D = 1$

$$D = \sum_{i=1}^{N}\frac{n_i}{N_{fi}} = 1 \tag{8}$$

The accuracy of the Palmgren-Miner rule has often being questioned (Ibrahim and Miller 1979; Miller and Ibrahim 1981; Miller et al. 1986). First, the assumption that damage accumulates

proportionally at all stress levels was deemed to be simplistic, but tests have shown that it is conservative. Second, for high-cycle fatigue, the Palmgren-Miner rule results in overestimated life prediction, but it fails to consider the damage that may accumulate when damage induced during large-amplitude cycles increases during cycles of amplitudes below the fatigue limit (using a fatigue life curve that has been developed for constant amplitude cycles). However, this is of little consequence in low-cycle fatigue, and usefulness of this simple analytical criterion remains of considerable value and is suitable for the application considered (Sobczyk 1989).

A simple example of the stress–strain curve in Fig. 4 presents the methodology mentioned previously, and the difference between the three fatigue life calculation methods in Tables 1–3. The strain range of 0.03 and stress range of 736.4 MPa (106.8 ksi) from Point A to Point B in Fig. 4 was considered to contribute half of the cycle in Tables 1–3. By solving Eq. (5), the resulting value of $2N_f$ is 852 reversals using the Basquin-Coffin-Manson method. Consequently, N_{fi} is 426 reversals (or cycles) to failure if the stress range from Point A to Point B was continuously repeated. The damage for the half cycle of that strain range from Point A to Point B is obtained by dividing 0.5 by 426, resulting in the damage value of 0.00117. Similarly, steps were taken for all other strain ranges from Point B to Point I in Fig. 4, and the total damage D of 0.05497 was obtained by summing the contributions from each cycle. The fatigue life for that repeated strain history is then calculated by taking the reciprocal of the total damage, which gave 18.19 repetitions. For the Smith-Watson-Topper and Morrow approaches, steps taken to calculate the damages for each cycle and to estimate the fatigue life are similar to those in the Basquin-Coffin-Manson approach. The only difference lies in the formulas used; the Smith-Watson-Topper method considers a correction based on the maximum stress $\sigma_{\max}$, whereas the Morrow method uses mean stress σ_m to estimate the total life reversals of $2N_f$.

Strain History Calculation

In this study, the bridge superstructure was assumed to have simply supported steel girders and composite concrete deck, with the BRB connecting the abutment to the bridge superstructure along the bridge's longitudinal direction. The bridge total span length is L, with the bridge effective length of L_1 (equal to the distance from the BRB's attachment point along the girder to the fixed bearing at the far end of the span), the BRB's total length is L_2, and the end-offset length is a, as presented in Fig. 6(a). The reference temperature, T_r, was assumed to be the temperature when the BRB was first installed in the bridge. The temperature change, Δ_T, was considered to uniformly affect the entire bridge superstructure, and it corresponds to the reference temperature T_r subtracted by the recorded temperature T in one day (a sign convention was chosen so that a positive Δ_T would correspond to tension in the BRB). The values of T_r changed between the recorded maximum and minimum temperature at the specific bridge location, varying by 10°F intervals.

Uniform temperature changes Δ_T cause thermal expansions or contractions of the bridge and BRB. Positive Δ_T expands the bridge with an effective length L_1 resulting in elongation on the BRB, whereas negative Δ_T contracts the bridge causing the BRB in compression. As the T_r increased, BRB would experience more tensile strains than compressive strains, and vice versa. If the BRB's thermal deformation is ignored, then the thermal deformation of the bridge, δ, is equal to the displacement applied to the BRB, δ_{eq}, as illustrated in Fig. 6(a). Assuming that this displacement is only distributed inside the BRB core plate with the assumed length of cL_2, the strain in the BRB core plate can be simplified as

Table 1. Fatigue life calculation using the Basquin-Coffin-Manson method [Eq. (5)]

Point	From	To	$\Delta\varepsilon$	$\Delta\varepsilon/2$	$2N_f$	N_{fi}	n_i	$D_i = n_i/N_{fi}$
A to B	−0.02	0.01	0.03	0.015	852.4	426.2	0.5	0.00117
B to C	0.01	−0.03	0.04	0.02	423.2	211.6	0.5	0.00236
C to D	−0.03	0.05	0.08	0.04	81.8	40.9	0.5	0.01221
D to G	0.05	−0.04	0.09	0.045	62.2	31.1	0.5	0.01607
E to F	−0.01	0.03	0.04	0.02	423.2	211.5	1	0.00473
G to H	−0.04	0.04	0.08	0.04	81.8	40.9	0.5	0.01221
H to I	0.04	−0.02	0.06	0.03	160.8	80.4	0.5	0.00622

Note: Fatigue life, $N_f = 1/D = 18.19$; and total damage, $D = 0.05497$.

Table 2. Fatigue life calculation using the Smith-Watson-Topper method [Eq. (6)]

Point	From	To	$\Delta\varepsilon$	$\Delta\varepsilon/2$	$\sigma_{\max}$	$2N_f$	N_{fi}	n_i	$D_i = n_i/N_{fi}$
A to B	−0.02	0.01	0.03	0.015	333	1291.2	645.6	0.5	0.00077
B to C	0.01	−0.03	0.04	0.02	333	755.6	377.8	0.5	0.00132
C to D	−0.03	0.05	0.08	0.04	519.7	95.6	47.8	0.5	0.01046
D to G	0.05	−0.04	0.09	0.045	519.7	77.4	38.7	0.5	0.01291
E to F	−0.01	0.03	0.04	0.02	449.4	435.4	217.7	1	0.00459
G to H	−0.04	0.04	0.08	0.04	484.5	108.4	54.2	0.5	0.00922
H to I	0.04	−0.02	0.06	0.03	484.5	181.7	90.8	0.5	0.0055

Note: Fatigue life, $N_f = 1/D = 22.37$; and total damage, $D = 0.0447$.

Table 3. Fatigue life calculation using the Morrow method [Eq. (7)]

Point	From	To	$\Delta\varepsilon$	$\Delta\varepsilon/2$	σ_m	$2N_f$	N_{fi}	n_i	$D_i = n_i/N_{fi}$
A to B	−0.02	0.01	0.03	0.015	−35.1	862.6	431.3	0.5	0.00116
B to C	0.01	−0.03	0.04	0.02	−58.1	430	215	0.5	0.00232
C to D	−0.03	0.05	0.08	0.04	35.2	81.4	40.7	0.5	0.01228
D to G	0.05	−0.04	0.09	0.045	17.6	62	31	0.5	0.01612
E to F	−0.01	0.03	0.04	0.02	58.1	416.5	208.2	1	0.0048
G to H	−0.04	0.04	0.08	0.04	0	81.8	40.9	0.5	0.01222
H to I	0.04	−0.02	0.06	0.03	35.2	159.7	79.8	0.5	0.00626

Note: Fatigue life, $N_f = 1/D = 18.19$; and total damage, $D = 0.05516$.

$$\varepsilon_{eq} = \frac{\delta_{eq}}{c\ L_2} = \frac{\alpha_1 \Delta_T L_1}{c\ L_2} \tag{9}$$

where L_2 = total length of the BRB; α_1 = coefficient of thermal expansion of concrete taken as 0.000006 m/m/°F; and c = core plate yielding length ratio of the BRB. Note that the thermal expansion coefficient of steel (for the bridge girders) is 0.0000065 m/m/°F, which would have given slightly larger deformations. The thermal expansion coefficient for concrete was used based on the arbitrary assumption that the concrete deck cross sectional area for the bridge would be larger than the section area of steel girder and may govern thermal elongation.

More precisely, the effect of thermal changes in deforming the BRB itself should be considered. The stiffness of the BRB also needs to be taken into account, as well as its yield strength, P_y, which is defined later in this section. The thermal changes can cause not only elastic but also plastic deformations on the BRB. Next are four cases in which strains in the BRB core plate are derived considering deformations due to thermal expansion of only the bridge (i.e., Cases 1 and 3), or both the bridge and BRB (i.e., Cases 2 and 4). The BRB thermal deformations in the elastic (i.e., Cases 1 and 2) and plastic ranges (i.e., Case 3 and 4) are both investigated.

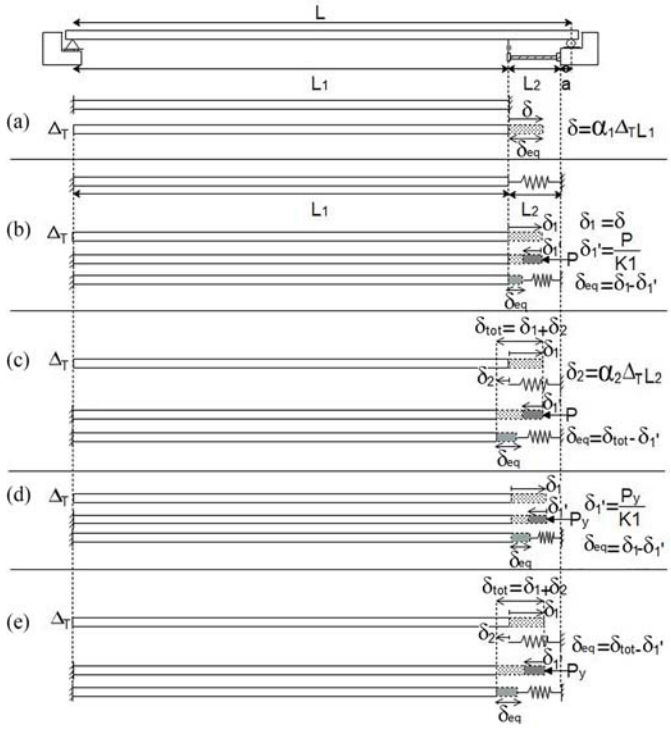

Fig. 6. Model for BRBs connecting bridge abutment and girder for calculating impact of bridge thermal expansion considering (a) only BRB stiffness; (b) BRB and bridge elastic stiffnesses; (c) BRB elastic stiffness and deformation of BRB due to temperature changes; (d) BRB plastic resistance to thermal expansion; and (e) force applied to the bridge due to the BRB's plastic resistance to thermal expansion and deformation of the BRB due to temperature changes.

Four Cases in Calculating the Strain History

Case 1: Elastically Calculated Strain History of BRBs (BRB Thermal Expansion = 0)

The BRB connecting to the bridge is simplified as an equivalent spring, as given in Fig. 6(b). Because of the high in-plane rigidity of the superstructure deck in the model considered, no significant rotations about a vertical axis are considered at the ends of the span. Although small rotations about a vertical axis could occur there due to seismic excitation in the bridge's transverse direction (resulting in slightly larger ductility demands), these are not foreseen to occur due to thermal effects; if this was a concern, the longitudinal BRBs could be installed near the midwidth of the superstructure to minimize the effect of these rotations. With respect to possible rotations about a horizontal axis, if this was a concern, longitudinal BRBs across the expansion joint of the bridge could be installed horizontally to minimize the effect of this rotation. In all cases, it remains that the simplified model is sufficient to generate the displacement and strain demand due to this straight bridge's thermal expansion and contraction under temperature changes. Possible rotations at the end of the bridge span are not considered in this paper, and they may be investigated in future research using a full three-dimensional (3D) model of the bridge. Also, a spring with the property of the BRB's core plate was used to model the BRB in this simplified model. A detailed 3D model of the entire BRB (including modeling of its interiors as fabricated) was built in Abaqus version 6.13 and analyzed under the temperature-induced displacement history to ensure that the fatigue analyses results using the simpler "spring" model (accounting only for the core plate) gave representative results. Because the magnitude of the temperature-induced displacement history was relatively small (compared with seismic demands), the BRB was not subjected to extensive yielding. Therefore, even though the 3D model of the BRB may give more accurate results in some cases, the simplified model was used to generalize the fatigue analyses results. However, information on the 3D model cannot be disclosed given that the BRBs analyzed are proprietary products.

The bridge deck end connected to the BRB was considered free to deform laterally as presented in Fig. 6(b), and thermal changes Δ_T in the bridge result in an expansion of the bridge of δ_1. Deformation of the BRB due to Δ_T was neglected. Because of the BRB stiffness, an equivalent force, P, pushes the bridge, resisting its thermal expansion, resulting in the lateral deformation $\delta_1^{'}$ illustrated in Fig. 6(b). The deformation at equilibrium is δ_{eq}, given by

$$\delta_{eq} = \delta_1 - \delta_1' = \delta_1 - \frac{P}{K_1} \tag{10}$$

Because the bridge and BRB are connected in series, the equivalent force P is equal to the total force in the system due to thermal changes

$$P = K_{\text{tot}}\delta_1 = \frac{K_1 K_2}{K_1 + K_2}\delta_1 \tag{11}$$

where K_1 and K_2 = effective stiffness of bridge and the BRB. Therefore, the equivalent deformation of the BRB due to thermal changes can be written as

$$\delta_{eq} = \delta_1 - \frac{K_1 K_2}{K_1 + K_2}\delta_1 \frac{1}{K_1} = \delta_1\left[1 - \frac{K_2}{K_1 + K_2}\right] \tag{12}$$

By substituting Eq. (12) into Eq. (9), the thermal strain of the BRB is

$$\varepsilon_{eq} = \frac{\delta_{eq}}{cL_2} = \alpha_1 \Delta_T \frac{L_1}{cL_2}\left[1 - \frac{K_2}{K_1 + K_2}\right] \tag{13}$$

Case 2: Elastically Calculated Strain History of BRBs (BRB Thermal Expansion = δ_2)

In this case, thermal change Δ_T is assumed to deform both the bridge and the BRB, producing δ_1 and δ_2, respectively, which were added up to the total thermal expansion of δ_{tot}, as presented in Fig. 6(c). As illustrated in Fig. 6(c), the deformation at equilibrium δ_{eq} can be written as

$$\delta_{eq} = \delta_{\text{tot}} - \delta_1' = \delta_{\text{tot}} - \frac{P}{K_1} \tag{14}$$

where P = equivalent force in the system due to total thermal expansions of the bridge and BRB, calculated as

$$P = K_{\text{tot}}\delta_{\text{tot}} = \frac{K_1 K_2}{K_1 + K_2}\delta_{\text{tot}} \tag{15}$$

By substituting Eq. (15) into Eq. (14)

$$\delta_{eq} = \delta_{\text{tot}} - \frac{K_1 K_2}{K_1 + K_2}\delta_{\text{tot}} \frac{1}{K_1} = \delta_{\text{tot}}\left[1 - \frac{K_2}{K_1 + K_2}\right] \tag{16}$$

The thermal strain of the BRB can be calculated as

$$\varepsilon_{eq} = \frac{\delta_{eq}}{cL_2} = \frac{\alpha_1 \Delta_T L_1 + \alpha_2 \Delta_T L_2}{cL_2} \left[1 - \frac{K_2}{K_1 + K_2}\right] \quad (17)$$

where α_2 = thermal expansion coefficient of the BRB, which is taken as 0.0000065 in/in/°F.

Case 3: Plastically Calculated Strain History of BRBs (BRB Thermal Expansion = 0)

Similar to Case 1, thermal changes Δ_T cause the bridge deck to deform as illustrated in Fig. 6(d). Because of the BRB stiffness, an equivalent force, P, resists these elongations, resulting in lateral deformation of δ_1' under that force. However, when the BRB's plastic response is taken into account, the equivalent force P is now limited to P_y, which is equal to the product of the BRB yielding core plate cross sectional area, A_{ysc}, and core plate steel yield strength, F_y. The equivalent deformation, δ_{eq}, in Fig. 6(d) is

$$\delta_{eq} = \delta_1 - \delta_1' = \delta_1 - \frac{P_y}{K_1} = \delta_1 - \frac{A_{ysc} F_y}{K_1} \quad (18)$$

The thermal strain of the BRB is calculated as

$$\varepsilon_{eq} = \frac{\delta_{eq}}{cL_2} = \frac{\alpha_1 \Delta_T L_1 K_1 - A_{ysc} F_y}{K_1 L_2 c L_2} \quad (19)$$

Case 4: Plastically Calculated Strain History of BRBs (BRB Thermal Expansion = δ_2)

Similar to Case 2, thermal changes Δ_T is considered to deform both the bridge deck and the BRB, as presented in Fig. 6(e). The total deformation due to thermal changes Δ_T is taken as $\delta_1 + \delta_2$. From Fig. 6(e), the deformation at equilibrium δ_{eq} can be written as

$$\delta_{eq} = \delta_{\text{tot}} - \delta_1' = \delta_{\text{tot}} - \frac{P_y}{K_1} = \delta_{\text{tot}} - \frac{A_{ysc} F_y}{K_1} \quad (20)$$

where P_y, A_{ysc}, and F_y are the same as previously defined in Case 3.

The thermal strain of BRB is calculated as

$$\varepsilon_{eq} = \frac{\delta_{eq}}{cL_2} = \left(\alpha_1 \Delta_T L_1 + \alpha_2 \Delta_T L_2 - \frac{A_{ysc} F_y}{K_1}\right) / cL_2 \quad (21)$$

Example

A simple example of the BRB thermal strain calculation is conducted using the equations in each of the previously mentioned four cases. The results are compared to illustrate how different the BRB thermal strains are, particularly regarding the BRBs considered as either elastic or plastic for the sake of calculating thermal deformations. The bridge with a clear span length of L is subjected to thermal changes ΔT, which are taken from 10 to 100°F within 10°F intervals. The ratios of BRB length L_2 over bridge length L are taken as 1, 2, 3, and 4%, and the BRB core plate yielding length ratio c is taken as 0.5. Assumptions are made for bridge concrete deck properties, such as compressive strength, f_c', as 20.7 MPa (3,000 psi); elastic modulus, E_1, as 21,525 MPa (3,122 ksi); thermal expansion coefficient, α_1, as 0.000006 m/m/°F; and deck cross sectional area, A_1, as 2 m^2 (3,150 in^2). The material for the BRB steel core plate is ASTM A36 steel with elastic modulus, E_2, as 200,000 MPa (29,000 ksi); yield strength, F_y, as 248 MPa (36 ksi); thermal expansion coefficient, α_2, as 0.0000065 m/m/°F; and the yielding core plate cross sectional area, A_{ysc}, as 0.0026 m^2 (4 in^2). The thermal strains of the BRB calculated for a length ratio of L_2/L equal to 1 and 3% are given in Fig. 7, whereas the other cases corresponding to 2 and 4% are presented in Fig. S2. To illustrate the sensitivity of the results to the various assumptions, an example is taken for a bridge with a length ratio of L_2/L equal to 3% and ΔT equal to 40°F. The thermal strains calculated per Eqs. (9), (13), and (17) are 0.0160, 0.0123, and 0.0128, respectively. If calculated by Eqs. (19) and (21), the results would be 0.0153 and 0.0158, respectively. From these results, it can be observed that elastically calculated BRB thermal strain (accomplished by neglecting the deformation δ_1') given by Eq. (9) is only slightly different from the one calculated plastically using the more precise Eq. (21). Eqs. (9) and (21) are both retained for further calculations of BRB thermal strain in the rest of this study, recognizing that the use of Eq. (9) results in larger strains in the BRB, which will lead to a more conservative estimation of low-cycle fatigue life.

Detailed Analysis and Results

BRB strain histories corresponding to the temperature histories presented in Figs. 3 and S2 were calculated using the thermal strain equations presented previously. Because of the space constraints, an example of how the results are obtained is given for BRBs with thermal strain calculated using the recorded real temperature data only from Memphis, whereas the complete results for all selected locations can be found in Wei and Bruneau (2016). The appendix presents the comparison of fatigue life calculated using strain histories obtained per Eq. (9) for all the other cities considered in this study. The use of the simplified method given in Eq. (9) (neglecting the bridge's deformation δ_1' resulting from the BRB's force) was found to lead to a more conservative estimation of low-cycle fatigue life, with only a small difference from the one calculated using the more precise method given in Eq. (21) (considering δ_1' as well as the plastic deformation of BRBs due to thermal changes). For illustration purposes, the strain histories are provided only from Eq. (9) and their corresponding cycles resulting from the rainflow counting method. The resultant stress–strain relationships of BRBs generated from the Ramberg-Osgood and Morrow equations are also provided for the strain histories generated from Eq. (9). Low-cycle fatigue life results estimated based on the Basquin-Coffin-Manson, Smith-Watson-Topper, and Morrow methods are given for thermal strains calculated using both Eqs. (9) and (21) for comparison. Except for the first step in which the strain histories were generated, the software program Fatiga was used for conducting the rainflow counting, calculating the damage produced by each cycle, and for estimating the fatigue life of BRB. Suggestions on the length of BRBs required to prevent their potential failure due to low-cycle fatigue are provided by the authors at the end of this process.

In this study, the material used for the BRB's core plate was assumed to be ASTM A572 Gr 42. Because there is no significant difference in the fatigue resistance properties of constructional steel over the 248-MPa (36-ksi) to 689-MPa (100-ksi) yield strength range, the strain-life relationship of ASTM A36 steel in Fig. 5 is deemed to also apply to A572 Gr. 42, recognizing that larger bridge thermal displacements are required to exceed the yield strains compared with lower grade steels. As such, material properties for A36 steel were used in Fatiga, and the results obtained will be conservative when applied to BRBs with yielding core plates of other steel grades.

The assumptions and formulas used to calculate the thermal strains of BRBs are described in the previous section. For each temperature history, maximum and minimum daily temperatures were recorded, resulting in maximum and minimum BRB thermal strains each day. These daily maximum and minimum strains were then assembled together into one continuous strain history with 732 data

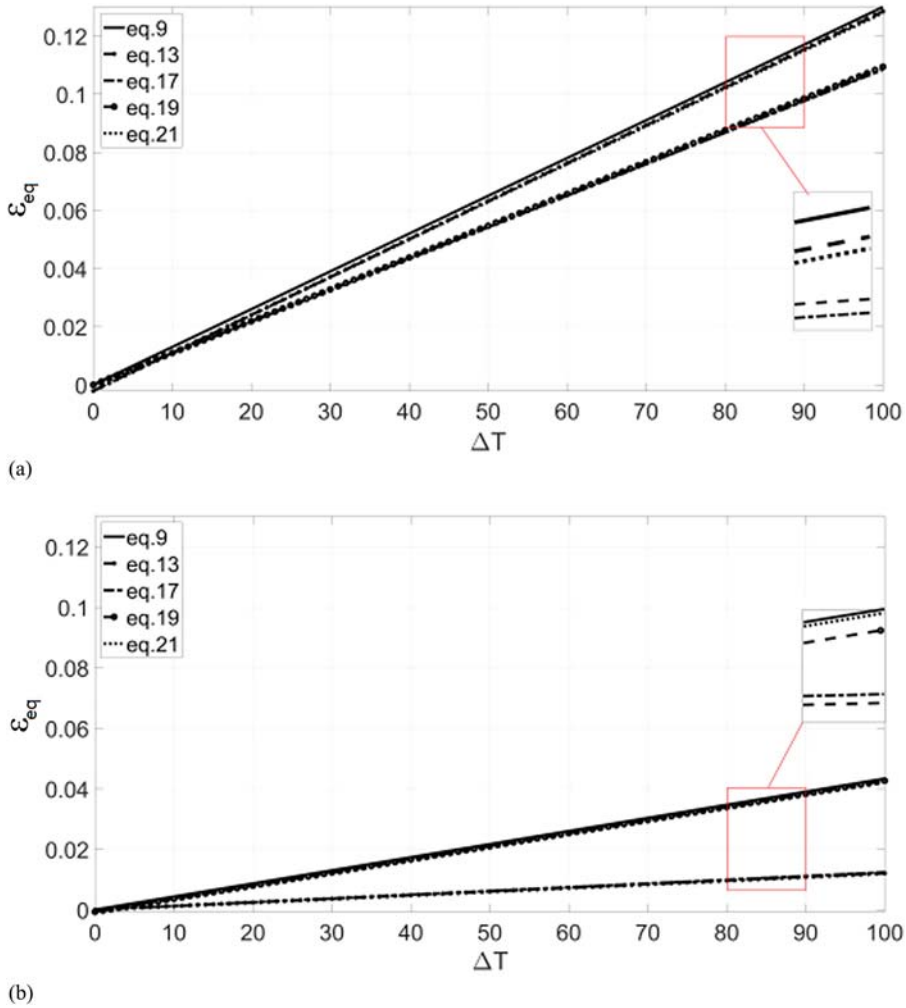

Fig. 7. Example of BRB thermal strain under various temperature changes in different cases (as the BRB length over the bridge length ratio changes): (a) $L_2/L = 1\%$; and (b) $L_2/L = 3\%$.

points spanning a full year with all its seasons (there were 366 days in 2012, the year for which the temperature values for different seasons were obtained).

The strain histories given in Figs. 8 and S3 provide the set of thermal strain histories calculated by Eq. (9) using recorded real-temperature data for a given year in Memphis in Fig. 3. The axis in the continuous thermal strain histories in Figs. 8 and S3 correspond to 732 data points associated with the strains calculated from the recorded maximum and minimum temperature within a year. For a given set of temperature data, increasing the reference temperature, T_r, causes the BRBs to experience more expansions/elongations and less contractions/shortening (and vice versa). Therefore, as illustrated in Figs. 8 and S3, BRBs have more tensile strains for $T_r = 100°\text{F}$ and more compressive strains for $T_r = 30°\text{F}$. Also, higher strains in the BRBs are found in the shorter core plate length of BRBs, i.e., in the smallest ratio between the BRB length and bridge total span length, and vice versa. Note that T_r was taken incrementally at 10°F, and only results for T_r corresponding to 30 and 100°F are presented in Fig. 8 due to space constraints. Similarly, the ratio L_2/L was taken incrementally from 1 to 6% at 1% intervals, and only results for 1 and 6% are given in Fig. 8 for comparisons. The other cases for 70°F and 3% are given in Fig. S3. The yielding length ratio of the BRB core plate c was kept constant at 0.5.

Low-cycle fatigue is identified by a small number of cycles with large plastic deformations in which the strain range, $\Delta\varepsilon$, is bigger than twice the yield strain ε_y, and this value is 0.00248 for A36 steel. Strain histories given in Fig. 8 demonstrate that the calculated thermal strains exceed 0.248% of strain at least for some cycles in most of the cases considered in the study (maximum strain is 9%), showing that the BRB at times would undergo high plastic strains, leading to the possibility of low-cycle fatigue failure.

The rainflow counting method was used in Fatiga to break the continuous strain history obtained from the temperature history into individual cycles. Stresses associated with the strains in each cycle were calculated by Fatiga to estimate the BRB fatigue life. The calculated stress with its associated strain, forming the cyclic stress–strain hysteresis loop, are plotted in Figs. 9(a–d), corresponding to the strain history in Figs. 8(a–d).

Recall that among these three methods chosen to calculate the fatigue life of BRB, the Basquin-Coffin-Manson method neglects the effect of mean stress σ_m, whereas both the Smith-Watson-Topper and Morrow methods consider the mean stress effect. The fatigue life reversals, $2N_f$, were obtained using all three methods for each cycle counted using rainflow counting. Damage given by each cycle D_i and the total damage D are obtained by using Eq. (8). The fatigue life was obtained by dividing the value of 1.0 by the total damage D. In the Palmgren-Miner rule, it is assumed that failure

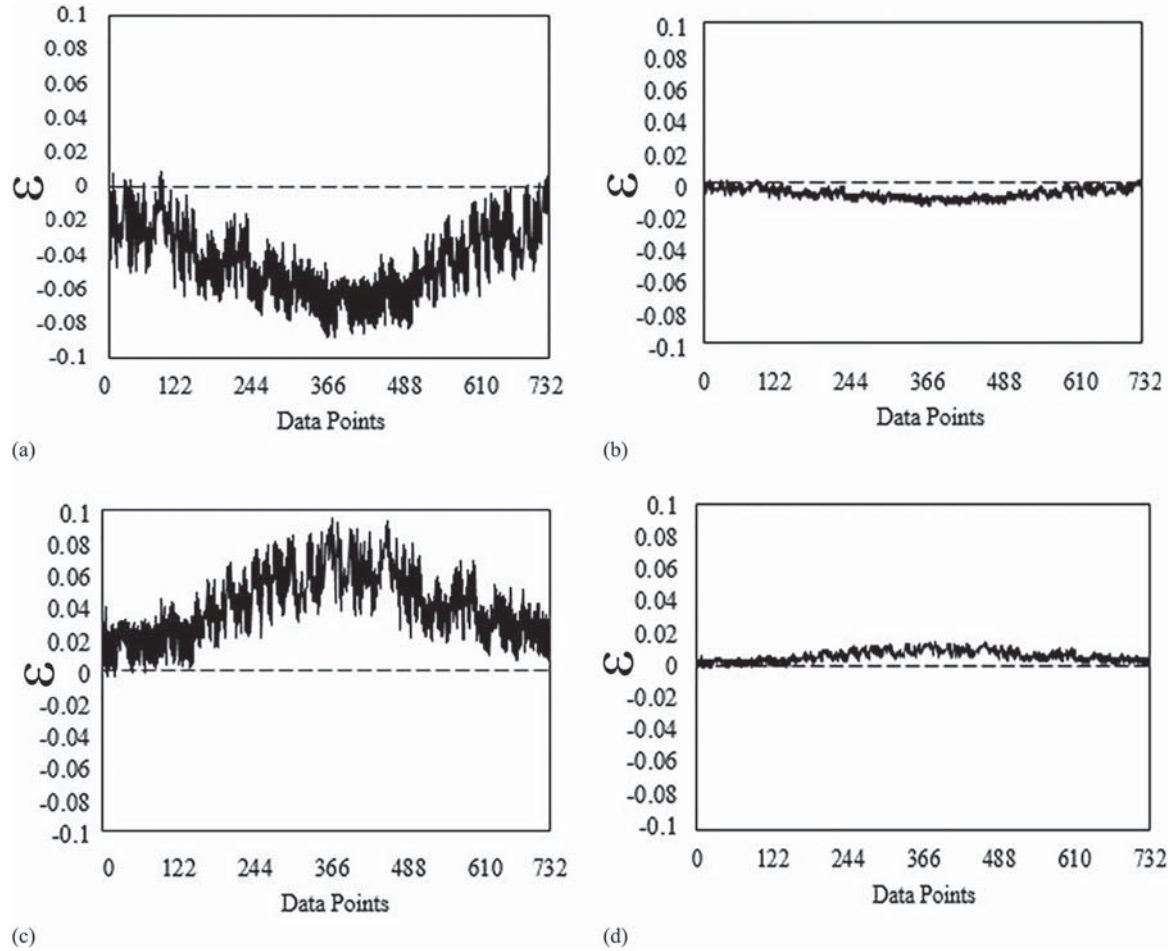

Fig. 8. Strain histories of BRBs for Memphis for (a) $T_r = 30°F$ and $L_2/L = 1\%$; (b) $T_r = 30°F$ and $L_2/L = 6\%$; (c) $T_r = 100°F$ and $L_2/L = 1\%$; and (d) $T_r = 100°F$ and $L_2/L = 6\%$.

occurs when the damage fraction reaches 1.0; therefore, the value of 1.0 is also synonymous to the attainment of fatigue life. The values of fatigue life are tabulated in Tables 4–9 for the reference temperature T_r of 30, 70, and 100°F because the percentages of L_{BRB}/L_{Bridge} changes for all nine cities. Low-cycle fatigue life results are presented for thermal strain histories calculated using Eqs. (9) and (21) to provide the comparison between the BRB's fatigue life estimation using a simplified approach [Eq. (9)] and precise method [Eq. (21)]. In places in which the fluctuation of temperature within a year was more severe (e.g., Memphis, Portland, and Quebec City), the calculated fatigue life of BRBs was less compared with places in which the yearly temperature variations were small (such as San Francisco and Charleston). At the BRB length ratio of $L_2/L = 6\%$, the fatigue life, N_f, of the BRBs exceeds the 75 years' design life for all reference temperatures, T_r, as well as for all three of the Basquin-Coffin-Manson, Smith-Watson-Topper, and Morrow methods considered in this study. The yielding length ratio of the BRB core plate is 0.5 in this case. Therefore, this initial analysis would suggest that the minimum ratio of the BRB core plate yielding length over the bridge length to avoid the low-cycle fatigue for all locations and reference temperature should at least be 3%.

To better visualize the difference in the fatigue life in Tables 4–9, the fatigue life of the BRBs are presented in Fig. 10 with the reference temperatures T_r of 100°F and BRB length ratio of L_{BRB}/L_{Bridge} as variables for Memphis. Similar fatigue life results are presented in Figs. S4 and S5 for T_r of 30 and 70°F. An expected design life of BRBs of 75 years, according to AASHTO (2014), is marked by the dashed line in Figs. 10(a and b). The longer the BRB is, the longer is the calculated fatigue life. Low-cycle fatigue life results in Figs. 10, S4, and S5 also show that the BRB's fatigue life calculated using the simplified approach [Eq. (9)] provides more conservative results than the precise approach [Eq. (21)] (i.e., shorter fatigue life results were obtained from the simplified approach). For example, in Fig. 10 for reference temperature T_r of 100°F, the low-cycle fatigue life results calculated by Eq. (9) are 183, 83.9, and 136 years using Basquin-Coffin-Manson, Smith-Watson-Topper, and Morrow methods, respectively. As for BRB low-cycle fatigue life calculated by Eq. (21), the results are 154, 72.9, and 115 years for all three methods. The low-cycle fatigue life predicted by the precise method is only approximately 1.7, 2.6, and 0.8% higher than the one calculated from the simplified approach [Eq. (9)] for Basquin-Coffin-Manson, Smith-Watson-Topper, and Morrow methods, respectively.

The BRB low-cycle fatigue life results also show that with an increase in T_r shorter fatigue life was obtained using the Smith-Watson-Topper method compared with the Basquin-Coffin-Manson and Morrow methods. Conversely, as T_r declines, more compressive strains were calculated in the BRB, resulting in bigger fatigue life estimated by the Smith-Watson-Topper method compared with the Basquin-Coffin-Manson and Morrow methods. For example, consider a BRB length ratio at $L_2/L = 6\%$ in Figs. 10, S4, and S5 in which the thermal strain is calculated using Eq. (9). The result shows that

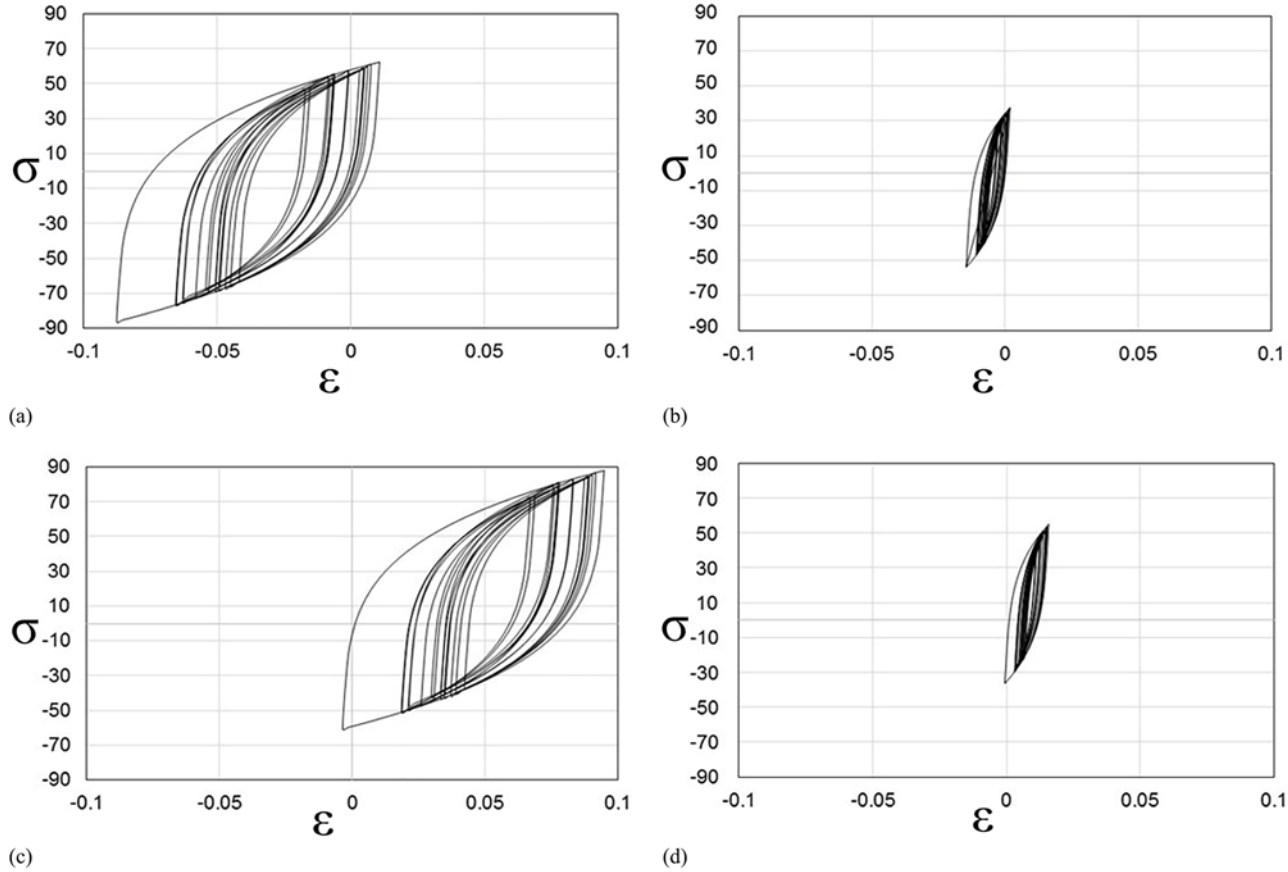

Fig. 9. Stress–strain relationship of BRBs for Memphis with (a) $T_r = 30°F$ and $L_2/L = 1\%$; (b) $T_r = 30°F$ and $L_2/L = 6\%$; (c) $T_r = 100°F$ and $L_2/L = 1\%$; and (d) $T_r = 100°F$ and $L_2/L = 6\%$ (stress unit: ksi).

Table 4. Fatigue life of BRBs using the Basquin-Coffin-Manson method with thermal strain data calculated by Eq. (9)

	$T_r = 100°F$						$T_r = 70°F$						$T_r = 30°F$					
	L_2/L (%)						L_2/L (%)						L_2/L (%)					
Location	1	2	3	4	5	6	1	2	3	4	5	6	1	2	3	4	5	6
Anchorage	—	—	—	—	—	—	3	17	50	111	102	137	3	17	50	111	102	137
Boston	—	—	—	—	—	—	2	13	37	81	151	183	2	13	36	79	147	174
Charleston	—	—	—	—	—	—	4	24	74	169	329	412	—	—	—	—	—	—
Los Angeles	2	11	35	80	172	183	2	11	33	75	146	183	—	—	—	—	—	—
Memphis	2	8	25	55	105	183	2	8	25	55	105	183	2	8	25	55	105	183
Portland	2	11	33	73	151	174	2	11	31	68	128	174	2	11	30	67	127	166
Quebec City	—	—	—	—	—	—	1	7	20	43	86	110	1	7	20	43	86	110
San Francisco	—	—	—	—	—	—	5	31	98	234	515	641	—	—	—	—	—	—
Seattle	—	—	—	—	—	—	3	17	52	118	253	366	3	17	52	118	253	366

increasing T_r affects the low-cycle fatigue life of BRBs calculated by the Smith-Watson-Topper method significantly compared with the other two methods. In Fig. S4, where $T_r = 30°F$, the results of the calculated fatigue life are 183, 3,320 and 252 years, whereas for $T_r = 100°F$ in Fig. 10, the fatigue lives are obtained as 171, 81.9, and 129 years for the Basquin-Coffin-Manson, Smith-Watson-Topper, and Morrow methods, respectively. This difference is expected because the Smith-Watson-Topper method predicts an infinite fatigue life if the maximum tensile stress is zero or negative, whereas the Morrow method provides more accurate results in compressive loadings. As for the Basquin-Coffin-Manson method, it generates almost a similar fatigue life with the different reference temperature, T_r, because the only parameter affecting the fatigue life is its strain ranges.

Calibration Factor Based on Experimental Results

In the past, the low-cycle fatigue behavior of BRBs was conducted under strain-controlled loading histories. The applied strains to BRBs would cause the local buckling of the encased core plate because the core plate is allowed to buckle first in the weak-axis bending direction due to the gap with the steel casing, which

Table 5. Fatigue life of BRBs using the Smith-Watson-Topper method with thermal strain data calculated by Eq. (9)

	$T_r = 100°F$						$T_r = 70°F$						$T_r = 30°F$					
	L_2/L (%)						L_2/L (%)						L_2/L (%)					
Location	1	2	3	4	5	6	1	2	3	4	5	6	1	2	3	4	5	6
Anchorage	—	—	—	—	—	—	2	10	27	52	58	59	5	26	72	172	271	384
Boston	—	—	—	—	—	—	2	11	31	66	120	133	13	65	173	361	640	828
Charleston	—	—	—	—	—	—	4	24	69	151	282	308	—	—	—	—	—	—
Los Angeles	1	6	17	37	47	59	2	12	36	80	153	230	—	—	—	—	—	—
Memphis	1	5	14	29	51	84	2	10	26	55	101	167	27	152	444	992	1,910	3,320
Portland	1	6	17	35	44	50	3	10	28	61	114	157	610	613	2,059	5,278	11,689	14,940
Quebec City	—	—	—	—	—	—	1	5	14	28	50	60	3	15	40	81	141	166
San Francisco	—	—	—	—	—	—	4	22	66	151	296	513	—	—	—	—	—	—
Seattle	—	—	—	—	—	—	2	13	38	83	158	205	117	783	2,713	7,264	1,6630	20,700

Table 6. Fatigue life of BRBs using the Morrow method with thermal strain data calculated by Eq. (9)

	$T_r = 100°F$						$T_r = 70°F$						$T_r = 30°F$					
	L_2/L (%)						L_2/L (%)						L_2/L (%)					
Location	1	2	3	4	5	6	1	2	3	4	5	6	1	2	3	4	5	6
Anchorage	—	—	—	—	—	—	3	14	41	91	68	127	3	19	55	125	233	242
Boston	—	—	—	—	—	—	2	13	37	78	147	157	3	16	47	106	199	203
Charleston	—	—	—	—	—	—	4	25	77	172	341	373	—	—	—	—	—	—
Los Angeles	2	9	26	59	103	109	2	11	33	79	151	161	—	—	—	—	—	—
Memphis	1	7	20	43	80	136	2	8	24	55	102	176	2	10	32	73	143	252
Portland	2	9	25	55	94	104	2	10	30	69	132	137	2	14	43	98	196	204
Quebec City	—	—	—	—	—	—	1	6	18	37	68	70	1	8	22	49	91	95
San Francisco	—	—	—	—	—	—	15	97	326	826	1,800	2,350	21	152	560	1,550	3,270	3,800
Seattle	—	—	—	—	—	—	3	16	47	107	215	231	4	22	72	181	345	351

Table 7. Fatigue life of BRBs using the Basquin-Coffin-Manson method with thermal strain data calculated by Eq. (21)

	$T_r = 100°F$						$T_r = 70°F$						$T_r = 30°F$					
	L_2/L (%)						L_2/L (%)						L_2/L (%)					
Location	1	2	3	4	5	6	1	2	3	4	5	6	1	2	3	4	5	6
Anchorage	—	—	—	—	—	—	3	16	44	91	160	172	3	19	54	113	202	227
Boston	—	—	—	—	—	—	3	16	45	95	174	181	3	15	42	91	167	179
Charleston	—	—	—	—	—	—	5	32	96	218	418	426	—	—	—	—	—	—
Los Angeles	2	11	32	71	136	145	3	15	46	105	203	208	—	—	—	—	—	—
Memphis	2	8	23	50	92	154	2	8	23	50	92	154	2	8	23	50	92	154
Portland	2	11	30	65	120	136	3	14	40	89	167	181	2	11	33	71	134	145
Quebec City	—	—	—	—	—	—	1	8	22	45	82	82	1	8	22	47	86	91
San Francisco	—	—	—	—	—	—	6	37	119	284	572	589	—	—	—	—	—	—
Seattle	—	—	—	—	—	—	4	21	64	144	280	290	3	17	52	118	226	245

produces additional flexural plastic deformations and strains in addition to the pure axial strains in the calculation of the BRB's thermal strains used in the previous section (Tsai et al. 2014). Therefore, a calibration factor is necessary to consider that the local buckling of BRBs may reduce the estimated low-cycle fatigue life results presented previously. This calibration factor is expected to depend on how the BRB is fabricated because this would have an impact on the amplitude of the local buckles in the BRB core (Takeuchi et al. 2008). The calibration factors are only applicable to the type of BRBs used in the specific development.

Because little data are available for the low-cycle fatigue of BRBs under variable amplitude loading, the calibration is made only from the constant amplitude loading obtained from the four experiments by Usami et al. (2011), Wang et al. (2012a, b), Nakamura et al. (2000), and Maeda et al (1998). The two BRB types are built with different JIS steel grades in the core plate and the corresponding steel properties are compared with ASTM 36 steel grade in Table 10. Experiments by Nakamura et al. (2000) and Maeda et al (1998) also included some BRB specimens that used a special low-yield steel that can develop 40% elongation at failure and had a different low-cycle fatigue life. Therefore, data

Table 8. Fatigue life of BRBs using the Smith-Watson-Topper method with thermal strain data calculated by Eq. (21)

	$T_r = 100°F$						$T_r = 70°F$						$T_r = 30°F$					
	L_2/L (%)						L_2/L (%)						L_2/L (%)					
Location	1	2	3	4	5	6	1	2	3	4	5	6	1	2	3	4	5	6
Anchorage	—	—	—	—	—	—	2	9	24	47	79	83	5	26	68	133	224	256
Boston	—	—	—	—	—	—	2	12	32	67	117	121	16	78	203	401	678	832
Charleston	—	—	—	—	—	—	5	28	78	168	302	369	—	—	—	—	—	—
Los Angeles	1	6	17	34	60	63	2	12	34	76	143	266	—	—	—	—	—	—
Memphis	1	5	13	26	46	73	2	8	22	46	82	133	34	197	573	1,260	2,340	3,960
Portland	1	6	16	32	56	60	3	9	24	52	95	133	614	1,178	4,631	1,3466	31,553	55,440
Quebec City	—	—	—	—	—	—	1	5	14	28	48	51	5	17	42	83	140	166
San Francisco	—	—	—	—	—	—	4	41	110	162	312	633	—	—	—	—	—	—
Seattle	—	—	—	—	—	—	3	15	42	90	166	211	161	1,206	4,695	14,014	35,556	41,583

Table 9. Fatigue life of BRBs using the Morrow method with thermal strain data calculated by Eq. (21)

	$T_r = 100°F$						$T_r = 70°F$						$T_r = 30°F$					
	L_2/L (%)						L_2/L (%)						L_2/L (%)					
Location	1	2	3	4	5	6	1	2	3	4	5	6	1	2	3	4	5	6
Anchorage	—	—	—	—	—	—	3	13	36	73	122	134	3	18	51	106	184	191
Boston	—	—	—	—	—	—	3	14	39	82	145	152	3	16	47	99	189	213
Charleston	—	—	—	—	—	—	5	29	88	196	377	428	—	—	—	—	—	—
Los Angeles	2	9	25	53	96	105	2	11	32	69	133	153	—	—	—	—	—	—
Memphis	1	7	19	39	70	115	1	7	19	41	76	125	2	10	30	67	126	213
Portland	2	9	24	50	87	91	2	9	25	55	102	111	2	14	40	90	167	192
Quebec City	—	—	—	—	—	—	1	7	18	36	64	95	2	8	22	47	85	114
San Francisco	—	—	—	—	—	—	5	31	99	231	464	532	—	—	—	—	—	—
Seattle	—	—	—	—	—	—	3	18	54	120	230	266	3	21	65	149	297	320

for BRBs with this special steel were excluded in this study. Every type of BRB manufacturing detail is not shown in this study due to space constraints.

The low-cycle fatigue experiments were conducted under a constant amplitude loading test with the loading protocol illustrated in Fig. 11. The experiments were conducted by first controlling the axial displacement up to the yield displacement of BRBs, δ_y. Then, the constant strain amplitude, $\Delta\varepsilon/2$, specified in Table 11 was imposed cyclically, starting with tensile strains followed by compressive strains, until the BRB specimens failed. In each case, the number of cycles to the failure of BRBs used in the experiments, N_{f_a}, are given in Table 11. The number of cycles to failure for the constant strain amplitude, $\Delta\varepsilon/2$, specified in Table 11 are calculated using the Basquin-Coffin-Manson method, and the steel fatigue properties of ASTM A36 were used. The resulting fatigue life calculated using the Basquin-Coffin-Manson method, N_{f_b}, was compared by taking the ratio with N_{f_a}, as given in Table 11. The Basquin-Coffin-Manson method was used because it ignores mean stress correction, which is consistent with the way the provided fatigue life was calculated in the literature on prior BRB tests.

Regression analysis was conducted to obtain the calibration factors by comparing the plot of the relationship between the strain amplitude, $\Delta\varepsilon/2$, and the number of failure cycles, N_f, for the experimental results and for the predicted values using the Basquin-Coffin-Manson method. The calibrations factors were categorized by the different steel grades.

For SM400A steel, the exponential regression for the fatigue life obtained using experimental results is

$$y = 317.27e^{-111.8x} \tag{22}$$

The exponential regression for the calculated fatigue life using the Basquin-Coffin-Manson method and ASTM A36 material fatigue properties is

$$y = 3068.3e^{-98.14x} \tag{23}$$

The two regression lines fitting the fatigue life results are illustrated in Fig. 12(a) (in log-linear space). A calibration factor, α, equal to 0.103, is calculated by scaling the straight lines as

$$\alpha(3068.3e^{-98.14x}) = 317.27 \tag{24}$$

Assume that the BRB low-cycle fatigue life calculated using the method in previous sections is 75 years. With the calibration factor of 0.1, the BRB would have to be periodically replaced (once every 7.5 years), or designed to have a longer core plate to achieve the same 75 years' fatigue life.

Similarly, for the SN400B steel, the regression lines for the fatigue life were obtained from both SN400B BRB experimental results and calculated values using the Basquin-Coffin-Manson method and ASTM A36 material fatigue properties, as presented in Eqs. (25) and (26), respectively. The calibration factor β_1 of 0.04 can be calculated from the regression curves in Fig. 12(b)

$$y = 0.0552x^{-2.218} \tag{25}$$

$$y = 0.0022x^{-2.477} \tag{26}$$

The strain amplitudes applied to the SN400B BRBs listed in Table 11 vary from elastic to plastic strain range. The calibration factor β_1 considers both the elastic and plastic strains range. Because the plastic strain amplitudes contribute more to the

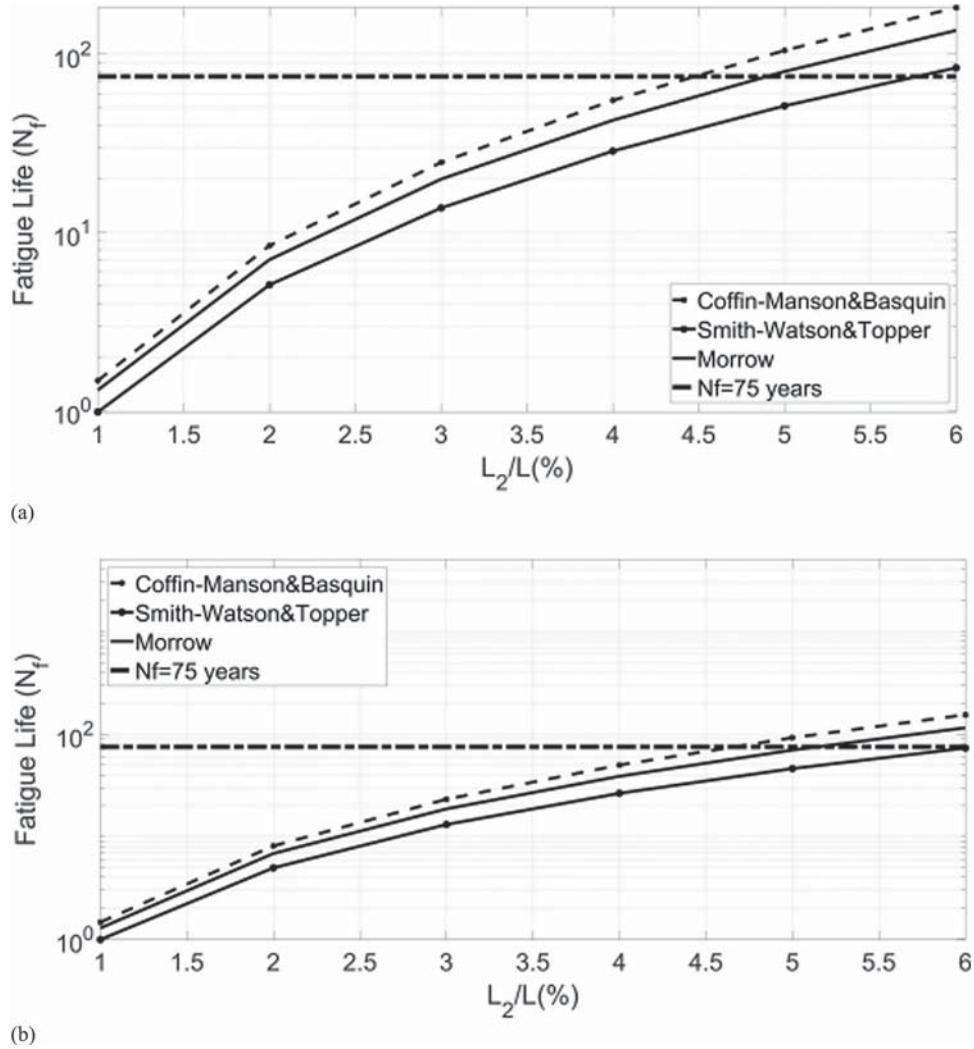

Fig. 10. Fatigue life of BRBs for Memphis with $T_r = 100°F$ calculated by (a) Eq. 9; and (b) Eq. 21.

Table 10. Material properties of ASTM A36, SM400A, and SN400B

Experiments by	Steel grade	Young's modulus [E (MPa)]	Yield strength [σ_y(MPa)]	Yield strain (ε_y)
Higashida et al. (1978)	ASTM A36	200,000	250	0.00124
Usami et al. (2011); Wang et al. (2012a)	SM400A	210,000	291	0.00139
Nakamura et al. (2000); Maeda et al. (1998)	SN400B	205,000	259	0.00126

fatigue life of the BRBs, another calibration factor was calculated corresponding to the strain amplitudes greater than 0.00124 (i.e., yield strain for A36 steel). Fig. 12(c) demonstrates the regression line comparisons for the plastic strain amplitudes, in which Eqs. (25) and (26) change to Eqs. (27) and (28) for the experimental results of SN400B and calculation values using the Basquin-Coffin-Manson method and ASTM A36 steel properties. The resulted calibration factor, β_2, is 0.33. Assuming that the BRB low-cycle fatigue life is 75 years, the BRB would have to be periodically replaced (once every 3 and 23 years corresponding to β_1 and β_2), or designed to have longer core plate to achieve the same 75 years' fatigue life

$$y = 93471e^{-449.8x} \tag{27}$$

$$y = 31596e^{-583.2x} \tag{28}$$

Because the calibration factors calculated for the two types of BRBs are quite different, while awaiting further experimental data it is recommended to use the calibration factor that gives more conservative results, which is 0.1. This calibration factor would significantly reduce the minimum BRB core plate length ratio required to avoid the low-cycle fatigue obtained in previous sections. Because this calibration factor would differ for different BRB manufacturers, low-cycle fatigue tests of BRBs should be conducted to quantify this value. Although this reduction of fatigue life was not incorporated in the recommended BRB core plate length ratio in the previous section, the method to obtain this factor was provided in this section.

Conclusions

Low-cycle fatigue analyses were conducted with various levels of refinements for BRBs installed across the expansion joint of bridges as part of the bidirectional EDSs. The fatigue life analyses results are compared and the following conclusions are made:

1. Assuming the deformation of BRBs due to thermal changes to be equal to the thermal expansion of the bridge (i.e., neglecting force applied to the bridge due to resistance to thermal expansion and deformation of BRBs due to temperature changes) would result in slightly larger strains in the BRB and provide more conservative estimation of low-cycle fatigue life of BRB.
2. Using the Smith-Watson-Topper method (which provided the most conservative low-cycle fatigue life of BRBs because this method accounted for the tensile mean stress in the low-cycle fatigue regime), and neglecting the BRB's core plate local buckling, the ratio of the BRB's length over bridge total length, L_2/L, should be 6% to satisfy the 75 years' design life as required by AASHTO without low-cycle fatigue failure (for the worst of all locations and installation temperatures considered). Assuming the BRB's core plate yielding length ratio to be 0.5, the minimum ratio of the BRB core plate yielding length over the bridge length should at least be 3%. This ratio is the projected length ratio of BRBs in the longitudinal direction over the bridge length, when the longitudinal BRBs are inclined.
3. The flexural strains introduced by local buckling of the BRB yielding core add flexural strains to the pure axial strains of the core plate inside the BRB. The comparison between past low-cycle fatigue experiment results on certain types of BRBs from the literature and the fatigue analysis results using the Basquin-Coffin-Manson method gave the calibration factors, which reduce the fatigue life and increase the required minimum BRB core plate yield length ratio. Calibration factors are expected to depend on how BRBs are fabricated. As such, values should be developed for the various designs offered by BRB manufacturers.

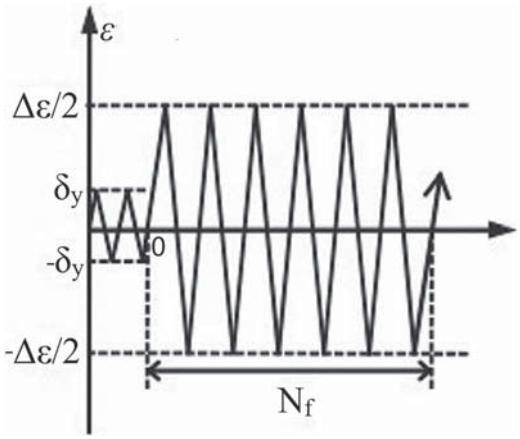

Fig. 11. Loading protocol of constant amplitude low-cycle fatigue test.

These conclusions are made focusing on the temperature-change effect on BRB design in bidirectional ductile diaphragm systems for seismic design consideration. Although the results are valuable, the findings are arguably subject to the limitations of this study, which include (1) the limited number of cities (and thus of temperature ranges) considered, (2) assumptions on the low-cycle behavior of BRBs (i.e., BRB characteristics change across different BRB manufacturers), and (3) the neglected possible impact of other factors on design. For example, designers should verify if the braking forces caused by the vehicular live load will yield the BRB or reduce the BRB's fatigue life significantly with the added stress cycles.

Along with the recommended BRB core plate length ratio limit, which is a useful parameter for designing BRBs in bidirectional ductile EDSs to ensure their long-term performance, this study also provides a controlling temperature-induced displacement history (i.e., the one that resulted in the smallest fatigue life for a given ratio of BRB core plate length). This information was used in combination with the seismic displacement demands to investigate the experimental performance of the BRBs under different displacement protocols considered. This experimental work, along with the information on BRB design and detailing recommendations for the current purpose, was presented in Wei and Bruneau (2018). Future study may investigate the effect of braking forces on the previously mentioned findings. This could be done considering dynamic

Table 11. BRB specimen test data and results under constant amplitude strain loading

Experiments by	Specimens	$\Delta\varepsilon/2$	Number of failure cycles (N_f)		N_{fa}/N_{fb}
			Experiment (N_{f_a})	BCM (N_{f_b})	
Maeda et al. (1998)	400-D1	0.0072	534	3,116	0.17
	400-D2	0.00485	1,481	7,484	0.20
	400-D3	0.00375	3,100	13,238	0.23
	400-D4	0.00285	8,650	24,330	0.35
	400-D5	0.00215	24,250	45,454	0.53
	400-L1	0.00085	63,900	355,961	0.18
	400-L2	0.000425	376,000	1,655,977	0.23
	400-L3	0.0003	1140,000	3,581,581	0.32
	400-L4	0.00017	5,350,000	12,655,943	0.42
Nakamura et al. (2000)	400-200	0.02	140	1,504	0.09
	400-150	0.015	211	2,847	0.07
	400-040	0.004	4,050	53,351	0.07
Usami et al. (2011)	FE-1.0	0.01	111	1,504	0.07
	FE-2.0	0.02	29	323	0.09
	FE-3.0	0.03	14	132	0.11
Wang et al. (2012b)	FE-4.0 (NS)	0.04	4	70	0.06
	FT-3.5 (NS)	0.035	5	94	0.05

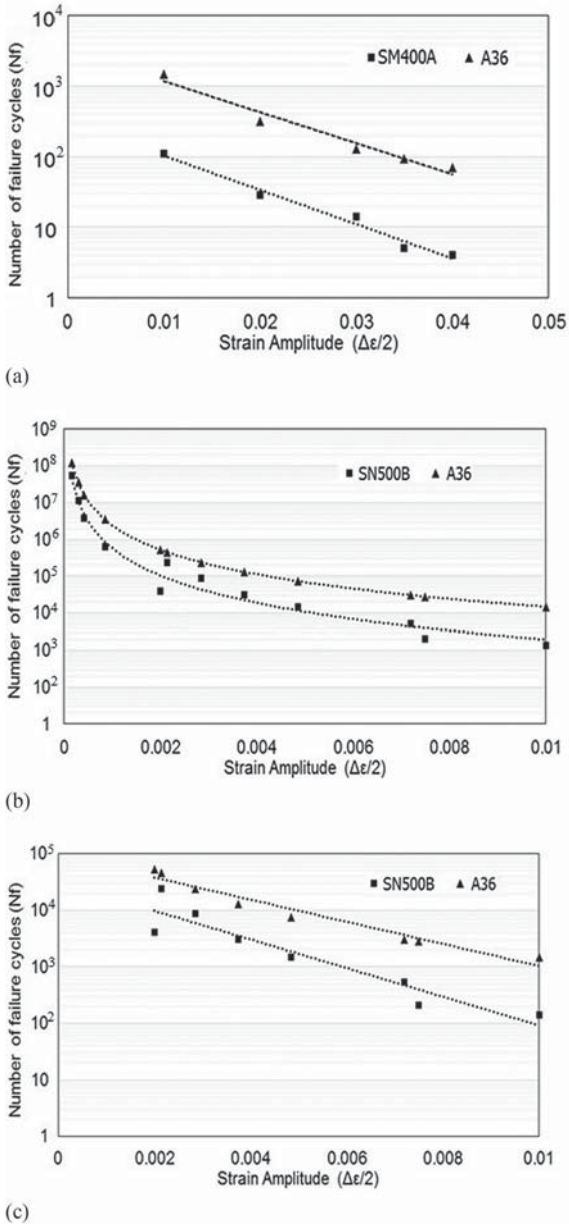

Fig. 12. Comparison of regression analysis results between fatigue life obtained from experiments and calculation using the Basquin-Coffin-Manson method: (a) SM400A; (b) SN500B; and (c) SN500B for plastic strain amplitude only.

analyses to compare those braking forces with the seismic force effects (which depend on the seismic hazard that varies across the country). A thorough investigation of the impact of this braking-force limit state also may be conducted on typical designs of BRBs to determine in which instances it could govern over the seismic limit state (possibly in a low seismic zone).

Appendix. Fatigue Life of BRBs for the Nine Cities Considered

The fatigue life of BRBs for the nice cities considered is based on strain history calculated per Eq. (9) for BRB versus bridge length ratios from 1 to 6% with installation temperatures at 100, 70, 30, and 0°F using the Basquin-Coffin-Manson method.

		Fatigue life (years)								
T_r (°F)	L_2/L (%)	a	b	c	d	e	f	g	h	i
100	1	—	—	—	2	2	2	—	—	—
	2	—	—	—	11	8	11	—	—	—
	3	—	—	—	35	25	33	—	—	—
	4	—	—	—	80	55	73	—	—	—
	5	—	—	—	172	105	151	—	—	—
	6	—	—	—	183	183	174	—	—	—
70	1	3	2	4	2	2	2	1	5	3
	2	17	13	24	11	8	11	7	31	17
	3	50	37	74	33	25	31	20	98	52
	4	111	81	169	75	55	68	43	234	118
	5	102	151	329	146	105	128	86	515	253
	6	137	183	412	183	183	174	110	641	366
30	1	3	2	—	—	2	2	1	—	3
	2	17	13	—	—	8	11	7	—	17
	3	50	36	—	—	25	30	20	—	52
	4	111	79	—	—	55	67	43	—	118
	5	102	147	—	—	105	127	86	—	253
	6	137	174	—	—	183	166	110	—	366
0	1	3	—	—	—	—	—	1	—	—
	2	17	—	—	—	—	—	7	—	—
	3	50	—	—	—	—	—	20	—	—
	4	111	—	—	—	—	—	43	—	—
	5	102	—	—	—	—	—	86	—	—
	6	137	—	—	—	—	—	110	—	—

Note: Row 2: (a) = Anchorage; (b) = Boston; (c) = Charleston; (d) = Los Angeles; (e) = Memphis; (f) = Portland; (g) = Quebec City; (h) = San Francisco; and (i) = Seattle; and the — = infinite life.

Acknowledgments

This study was sponsored by the Transportation Research Board of the National Academies under the TRB-IDEA Program (NCHRP-172). The authors acknowledge the oversight, valuable comments, and feedback from the NCHRP IDEA Project Advisor Lian Duan (California DOT), and the other members of the Project's Expert Advisory Panel, namely Geoffrey Swett and Bijan Khalegi (Washington DOT), Taneja Rajesh and Richard Marchione (New York DOT), Tom Ostrom (California DOT), and Phil Yen and Fred Faridazar (Federal Highway Administration). However, any opinions, findings, conclusions, and recommendations presented in this report are those of the writers and do not necessarily reflect the views of the sponsor.

Supplemental Data

Figs. S1–S5 are available online in the ASCE library (www.ascelibrary.org).

References

AASHTO. 2011. *AASHTO guide specifications for LRFD seismic bridge design.* 2nd ed. Washington, DC: AASHTO.

AASHTO. 2014. *AASHTO LRFD bridge design specifications.* 7th ed. Washington, DC: AASHTO.

AccuWeather. 2012. "US weather radar." Accessed June 1, 2014. http://www.accuweather.com/.

ASTM. 2017. *Standard practices for cycle counting in fatigue analysis.* ASTM E1049-85. West Conshohocken, PA: ASTM.

Basquin, O. 1910. "The exponential law of endurance tests." *ASTM Proc.* 10 (1910): 625–630.
Bruneau, M., C. M. Uang, and R. Sabelli. 2011. *Ductile design of steel structures*, 921. 2nd ed. Boston: McGraw-Hill.
Budaházy, V., and L. Dunai. 2015. "Numerical analysis of concrete filled buckling restrained braces." *J. Constr. Steel Res.* 115 (Dec): 92–105. https://doi.org/10.1016/j.jcsr.2015.07.028.
Celik, O., and M. Bruneau. 2011. "Skewed slab-on-girder steel bridge superstructures with bidirectional-ductile end diaphragms." *J. Bridge Eng.* 16 (2): 207–218. https://doi.org/10.1061/(ASCE)BE.1943-5592.0000141.
Clark, P., I. Aiken, K. Kasai, and I. Kimura. 2000. "Large-scale testing of steel unbonded braces for energy dissipation." In *Advanced technology in structural engineering*, edited by M. Elgaaly, 1–5. Reston, VA: ASCE.
Coffin, L. 1954. "A study of the effects of cyclic thermal stress on a ductile metal." *Trans. ASME* 76: 931–950.
Fahnestock, L., J. Ricles, and R. Sause. 2007. "Experimental evaluation of a large-scale buckling-restrained braced frame." *J. Struct. Eng.* 133 (9): 1205–1214. https://doi.org/10.1061/(ASCE)0733-9445(2007)133:9(1205).
Higashida, Y., J. D. Burk, and F. V. Lawrence. 1978. "Strain-controlled fatigue behavior of ASTM A36 and A514 grade-F steels and 5083-0 aluminum weld materials." *Weld J.* 57: 334–344.
Ibrahim, M., and K. Miller. 1979. "Determination of fatigue crack initiation life." *Fatigue Fract. Eng. Mater. Struct.* 2 (4): 351–360. https://doi.org/10.1111/j.1460-2695.1979.tb01093.x.
Iwata, M., T. Kato, and A. Wada. 2003. "Performance evaluation of buckling restrained braces in damage-controlled structures." In *Proc., 4th Int. Conf. Behavior of Steel Structures in Seismic Areas*, edited by F. Mazzolani, 37–43. Rotterdam, Netherlands: Balkema.
Koh, S. K., and R. I. Stephens. 1991. "Mean stress effects on low cycle fatigue for a high strength steel." *Fatigue Fract. Eng. Mater. Struct.* 14 (4): 413–428. https://doi.org/10.1111/j.1460-2695.1991.tb00672.x.
Korzekwa, A., and R. Tremblay. 2009. "Numerical simulation of the cyclic inelastic behaviour of buckling restrained braces." *Behaviour of steel structures in seismic areas*. London: Taylor & Francis.
López, W. A., and R. Sabelli. 2004. *Seismic design of buckling-restrained braced frames*. Steel Tips Rep. Lafayette, CA: Structural Steel Educational Council.
López-Almansa, F., J. C. Castro-Medina, and S. Oller. 2012. "A numerical model of the structural behavior of buckling-restrained braces." *Eng. Struct.* 41 (Aug): 108–117. https://doi.org/10.1016/j.engstruct.2012.03.045.
Maeda, Y., Y. Nakata, M. Iwata, and A. Wada. 1998. "Study on fatigue properties of axial-yield type hysteresis dampers." *J. Struct. Constr. Eng.* 63 (503): 109–115. https://doi.org/10.3130/aijs.63.109_1.
Manson, S. 1954. *Behavior of materials under conditions of thermal stress*. Rep. 1170. Washington, DC: National Advisory Committee for Aeronautics.
Marsh, M. L., and S. J. Stringer. 2013. *Performance-based seismic bridge design*. Washington, DC: National Academies Press.
Masing, G. 1926. "Eigenspannugen und Verfertigung bim Messing." In *Proc., 2nd Int. Congress on Applied Mechanics*, 332–335. Zürich, Switzerland: Int. Congress for Applied Mechanics.
Matsuishi, M., and T. Endo. 1968. *Fatigue of metals subjected to varying stress*, 37–40. Fukuoka, Japan: Japan Society of Mechanical Engineers.
Miller, K., and M. Ibrahim. 1981. "Damage accumulation during initiation and short crack growth regimes." *Fatigue Fract. Eng. Mater. Struct.* 4 (3): 263–277. https://doi.org/10.1111/j.1460-2695.1981.tb01124.x.
Miller, K., H. Mohamed, and E. de los Rios. 1986. "Fatigue damage accumulation above and below the fatigue limit." In *The behavior of short fatigue cracks*, 491–511. London: Mechanical Engineering Publications.
Miner, M. A. 1945. "Cumulative damage in fatigue." *J. Appl. Mech.* 12 (3): 159–164.
Morrow, J. 1968. "Fatigue properties of metals." *Fatigue design handbook*. New York: Society of Automotive Engineers.
Morrow, J. 1965. *Cyclic plastic strain energy and fatigue of metals, internal friction, damping, and cyclic plasticity*, 45–87. ASTM STP 378. Chicago: ASTM.
Nakagomi, T., T. Iwamoto, H. Kamura, H. Shimokawa, and K. Harayama. 2000. "Experimental study on fatigue characteristics of flat-bar brace with low yield stress steel stiffened by square steel tube." *J. Struct. Constr. Eng.* 65 (530): 155–161. https://doi.org/10.3130/aijs.65.155_2.
Nakamura, H., T. Takeuchi, Y. Maeda, Y. Nakata, T. Sasaki, M. Iwata, and A. Wada. 2000. *Fatigue properties of practical-scale unbonded braces*, 51–57. Nippon Steel Technical Rep. 82.
Osgood, C. C. 1982. *Fatigue design: International series on the strength and fracture of materials and structures*. 2nd ed. New York: Pergamon Press.
Palmgren, A. 1924. "Die lebensdauer von kugellagern." *Z. Ver. Dtsch. Ing.* 68 (14): 339–341.
Ramberg, W., and W. R. Osgood. 1943. *Description of stress-strain curves by three parameters*. Washington, DC: National Advisory Committee for Aeronautics.
Sabelli, R., S. Mahin, and C. Chang. 2003. "Seismic demands on steel braced buildings with buckling-restrained braces." *Eng. Struct.* 25 (5): 655–666. https://doi.org/10.1016/S0141-0296(02)00175-X.
Smith, K. N., P. Watson, and T. H. Topper. 1970. "A stress-strain function for the fatigue of metals." *J. Mater.* 4: 767–778.
Sobczyk, K. 1989. "Stochastic models for fatigue damage of materials." *Math. Comput. Modell.* 12 (8): 1046. https://doi.org/10.1016/0895-7177(89)90212-4.
Stephens, R. I., A. Fatemi, R. R. Stephens, and H. O. Fuchs. 2001. *Metal fatigue in engineering*. New York: John Wiley.
Takeuchi, T., M. Ida, S. Yamada, and K. Suzuki. 2008. "Estimation of cumulative deformation capacity of buckling restrained braces." *J. Struct. Eng.* 134 (5): 822–831. https://doi.org/10.1061/(ASCE)0733-9445(2008)134:5(822).
Tremblay, R., P. Bolduc, R. Neville, and R. DeVall. 2006. "Seismic testing and performance of buckling-restrained bracing systems." *Can. J. Civ. Eng.* 33 (2): 183–198. https://doi.org/10.1139/l05-103.
Tsai, K. C., B. C. Hsiao, J. W. Lai, C. H. Chen, M. L. Lin, and Y. T. Weng. 2003. "Pseudo dynamic experimental response of a full scale CFT/BRB composite frame." In *Proc., Joint NCREE/JRC Workshop on Int. Collaboration on Earthquake Disaster Mitigation Research*. Taipei, Taiwan: National Center for Research on Earthquake Engineering.
Tsai, K. C., A. C. Wu, C. Y. Wei, P. C. Lin, M. C. Chuang, and Y. J. Yu. 2014. "Welded end-slot connection and debonding layers for buckling-restrained braces." *Earthquake Eng. Struct. Dyn.* 43 (12): 1785–1807. https://doi.org/10.1002/eqe.2423.
Uang, C. M., M. Nakashima, and K. C. Tsai. 2004. "Research and application of buckling-restrained braced frames." *Int. J. Steel Struct.* 4 (4): 301–313.
Usami, T., C. Wang, and J. Funayama. 2011. "Low-cycle fatigue tests of a type of buckling restrained braces." *Procedia Eng.* 14: 956–964. https://doi.org/10.1016/j.proeng.2011.07.120.
Wang, C.-L., T. Usami, and J. Funayama. 2012a. "Evaluating the influence of stoppers on the low-cycle fatigue properties of high-performance buckling-restrained braces." *Eng. Struct.* 41 (Aug): 167–176. https://doi.org/10.1016/j.engstruct.2012.03.040.
Wang, C.-L., T. Usami, and J. Funayama. 2012b. "Improving low-cycle fatigue performance of high-performance buckling-restrained braces by toe-finished method." *J. Earthquake Eng.* 16 (8): 1248–1268. https://doi.org/10.1080/13632469.2012.703385.
Wei, X., and M. Bruneau. 2016. *Buckling restrained braces applications for superstructure and substructure protection in bridges*. Technical Rep. MCEER-16-0009. Buffalo, New York: MCEER.
Wei, X., and M. Bruneau. 2017. "Analytical investigation of buckling restrained braces' applications in bidirectional ductile end diaphragms for seismic performance of slab-on-girder bridge." *Eng. Struct.* 141 (Jun): 634–650. https://doi.org/10.1016/j.engstruct.2017.03.034.
Wei, X., and M. Bruneau. 2018. "Experimental investigation of buckling restrained braces for bridge bidirectional ductile end diaphragms." *J. Struct. Eng.* 144 (6): 04018048. https://doi.org/10.1061/(ASCE)ST.1943-541X.0002042.